Univerzita Karlova

Matematicko-fyzikální fakulta

HABILITAČNÍ PRÁCE

Charakterizace precipitačních procesů v Al(–Mn)–Sc–Zr a Mg–Tb(–Nd) slitinách a tenkých Pd–H filmech

RNDr. Martin Vlach, Ph.D.

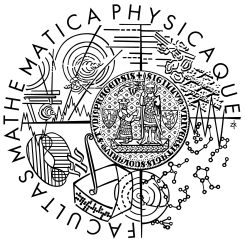

MATEMATICKO-FYZIKÁLNÍ FAKULTA
Univerzita Karlova

Praha, 2016

Charles University

Faculty of Mathematics and Physics

HABILITATION THESIS

CHARACTERIZATION OF PRECIPITATION PROCESS IN Al(–Mn)–Sc–Zr AND Mg–Tb(–Nd) ALLOYS AND THIN Pd–H FILMS

RNDr. Martin Vlach, Ph.D.

FACULTY
OF MATHEMATICS
AND PHYSICS
Charles University

Prague, 2016

Acknowledgement

I wish to express gratitude to my undergraduate and graduate supervisor, doc. RNDr. Ivana Stulíková, CSc., for her friendship, support, trust, patience and inspiring discussions. I would also like to thank all my colleagues and friends for their creativity, excellent work, and stimulating scientific discussions (doc. RNDr. Bohumil Smola, CSc., doc. Mgr. Jakub Čížek, Ph.D., RNDr. František Lukáč, Ph.D., RNDr. Marián Vlček, Ph.D., RNDr. Tomáš Kekule, Ph.D., RNDr. Petr Zinburg, Mgr. Hana Kudrnová, Mgr. Veronika Kodetová, Ing. Jaroslav Málek, Ph.D., Mst.-Sci. Ryota Gemma, Ph.D., Prof. Dr. Astrid Pundt, Mst.-Sci. Helmut Uchida, Ph.D., Mst.-Sci. Stefan Wagner, Ph.D., Hon.-Prof. Dr.-Ing. Volkmar Neubert, Dr.-Ing. Dhritti Tanprayoon, Ing. Vladivoj Očenášek, CSc., doc. RNDr. Pavel Svoboda, CSc., Mgr. Galina Kiryushina, Mgr. Tamara Čučková, RNDr. Naďa Žaludová, prof. RNDr. Ladislav Skrbek, DrSc. and Mgr. Luboš Veverka).

I would like to express my love to Ilona and thank her for constant support and understanding. I further thank all my co-workers from Media and Communications Office and Public Relations Office, as well as my students; without their contribution I would have never reached the results.

Some parts of this work were carried out with the efficient support of Czech Science Foundation (GAČR), The Grant Agency of the Academy of Sciences of the Czech Republic (GAAV) and Ministry of Education, Youth and Sports, Czech Republic (MŠMT) and The Alexander von Humboldt Foundation, Germany under the grants: GA106/04/1353 (GAČR), GA106/09/0407 (GAČR), GP P107/11/P201 (GAČR), 16-12828S (GAČR), KJB101120907 (GAAV), MSM0021620834 (MŠMT), MEB100915 (MŠMT) and MEB100912 (MŠMT). The work is a part of the activity of the Charles University Research Centre (UNCE) “Physics of Condensed Matter and Functional Materials.” The publications included in this work resulted from a fruitful collaboration with the Institute of Material Physics, University of Göttingen, Germany and Institut für Materialprüfung und Werkstofftechnik, Clausthal-Zellerfeld, Germany.

I hereby confirm that I wrote the habilitation thesis myself. All articles, internet sites, and other sources of information used are properly cited.

.....

Martin Vlach

Contents

Úvod/Preface

Habilitační spis je založen na kompilaci 23 recenzovaných článků v mezinárodních časopisech. Články reprezentují tři různé směry, kterými se dlouhodobě zabývám: a) precipitační procesy v hliníkových slitinách s přídavkem Sc a Zr, b) precipitační procesy ve slitinách hořčíku se vzácnými zeminami a c) vliv absorpce vodíku na fázové transformace v Pd filmech. Práce je tak rozdělena do tří základních kapitol dle problematiky. Habilitační spis uzavírá celkový přehled závěrů, použitá literatura, slovo autora a plné znění komentovaných článků (citovány a označeny jako [P]).

This habilitation thesis is based on a compilation of 23 peer-reviewed articles published in international journals. The papers represent my long-term research focus from three different angles: a) precipitation process in Al-based alloys with the content of Sc and Zr; b) precipitation process in Mg-based alloys with rare earths addition; and c) the influence of hydrogen absorption on phase transformation in Pd films. Therefore, this habilitation thesis is divided into three fundamental chapters according to their focus. The thesis is concluded by a summary of the achieved results, the full list of reference sources, the author's note and by the annotated and unabridged journal articles (marked and cited as [P]).

Role of the Sc and Zr addition in the selected Al-based alloys

Aluminium is the most used nonferrous metal; only the world's aluminium consumption increased year-on-year on average of 6%, largely driven by growth in China [1, 2]. The Al-based alloys are used in automobiles, other means of transport, and products with higher performance necessity, where they replace steel sheets and considerably reduce weight. According to the report of the European Aluminium Association (EAA), an intensive usage of aluminium would make it possible to decrease CO_2-emissions (decreasing weight of the car by about hundred kilograms reduces fuel consumption by about 5 % [3]). Although Al-based alloys have a long tradition of use especially as a lightweight material for traffic systems, trends in industry put a big emphasis on searching for ways to improve and stabilize the structure and properties of these materials through the careful control of thermo-mechanical processing schedules [4].

I. Ternary Al–Sc–Zr system

Scandium is the most effective element having an antirecrystallization impact in aluminium alloys [5, 6]. It increases recrystallization temperature of the material and thus products in the non-recrystallized state show improved strength properties [5–10]; it also has a beneficial effect on weldability and corrosion resistance [5, 6, 10]. The high influence of Sc on properties of the Al-based alloys is attributed to the high density of the Al_3Sc-dispersoids [4–15]. These particles precipitate as equilibrium phase and they are fully coherent to the matrix [4–6, 13, 14]. An attractive and veritable advantage is that the Al_3Sc phase does not change the material density and it is unusually stable with respect to coarsening – much higher than the commercial age-hardening 2xxx and 6xxx series alloys (containing Cu, Mg and Si) [4, 14–17].

The thermal stability of the Al_3Sc phase is further improved by addition of Zr [6, 10, 13]. Scandium atoms substitute zirconium atoms in the Al_3Zr phase and vice versa zirconium atoms for the Al_3Sc compound. Zr additions decrease the lattice parameter of the $Al_3(Sc,Zr)$ precipitates, and that decreases concomitantly the α-Al/$Al_3(Sc,Zr)$ interfacial misfit [6, 8–10]. The positive effect on recrystallization temperature, hardness, corrosion resistance and weldability attained due to the formation of a dense and homogeneous distribution of the $L1_2$-structured $Al_3(Sc,Zr)$ coherent precipitates is very pronounced [6, 10, 13–20]. Mechanical properties of the alloys with Sc and Zr content depend on their microstructure and phase composition, so their knowledge provides an opportunity to improve material properties by thermal treatment.

The complex nanostructure of the $Al_3(Sc,Zr)$ phase in aluminium has been discussed in several recent articles by studies using conventional microscopy and/or high-resolution transmission electron microscopy (HR-TEM) [18–21]. Atom-probe tomography (APT) was also employed to measure Sc,Zr-concentration and distribution [13, 20]. APT has shown that Sc-rich clusters can be formed in the early stages of precipitation above annealing temperatures of ~ 260 °C [13]. These clusters subsequently transform into the Al_3Sc particles with the $L1_2$ structure. When Zr diffusion becomes significant, Zr atoms are found to segregate to Al_3Sc/α-Al matrix interfaces. During further annealing (at ~ 400 °C) dispersoids with complex core–shell structure consisting of an Al_3Sc core embedded in an $Al_3(Sc,Zr)$ shell are developed [13, 20].

The decomposition sequence of oversaturated solid solution of the Al–Sc–Zr-based system is known in the form [P1, P2, 13, 20]: Sc-rich clusters → Al_3Sc phase → layer rich in Zr → $Al_3(Sc,Zr)$ phase.

Clusters in Al-based alloys can be universally very abundant and are known that they affect the resistivity. Many authors have aimed at explaining either the increase or decrease of resistivity at the beginning of the precipitation kinetics, showing that the resistivity change is associated with the existence of small clusters (e.g. Refs. [6, 12, 22]). Modelling the electrical resistivity evolution in the Al–Sc-based alloys using cluster dynamics predicted the time evolution of the size distribution supposing that the excess resistivity of atomic fraction of the clusters is proportional to the number density of the clusters, where the proportionality coefficient is being supposed constant and equals to the resistivity contribution of monomers [12]. The model assumes that the resistivity increase during coarsening arises mainly from large clusters ($n_{Sc} \geq 11$). However, any resistivity increase due to pre-precipitation stages has never been observed experimentally in the Al–Sc-based alloys, and only solutes and small clusters $n_{Sc} \leq 10$ (dimmers mainly) were present at most after short annealing times up to 10^4 s at temperatures below ~ 230 °C [12].

The author of this work and co-authors (e.g. Refs. [P1, P2]) observed even a small resistivity decrease connected with Sc atoms clustering at the beginning of supersaturated solid solution decomposition in the different types of the Al–Sc–Zr-based alloys after annealing up to ~ 210 °C. This behaviour of resistivity can be easily understood since the formation of small Sc clusters decreases the concentration of Sc solutes in the Al matrix. It is also worth noticing that the effect of thermal vacancies on the resistivity is too small to be detected up to ~ 400 °C [P2, 23, 24]. We have already provided measurements of the Al–Sc–Zr alloy which showed that the Al_3Sc-phase precipitation can start at ~ 220 °C and subsequent Zr-segregation to the Al_3Sc/α-Al matrix interfaces might take place already at ~ 240 °C [P1, P2]. The main resistivity decrease and main (micro)hardness (HV) increase in the Al–Sc–Zr system have their origin in these processes [P1–P3]. It was also shown that Sc atoms contribute to the growth of the Zr-rich shell in spite of substantial Sc depletion in the nearest neighbourhood of growing of the Al_3Sc dispersoids [P1, P2]. The apparent activation energy for precipitation of the Sc,Zr-containing particles through the decomposition sequence of the Al–Sc–Zr system was also calculated, see Refs. [P1, P4]. For the formation of the Al_3Sc particles approx. 120 kJ·mol^{-1} was determined, for the formation of a layer enriched in Zr atoms also approx. 120 kJ·mol^{-1} was calculated. Although the author and co-authors have performed several DSC measurements on the Al–Sc–Zr-based system, the apparent activation energy of 320 ± 96 kJ·mol^{-1} for the formation of the $Al_3(Sc,Zr)$ phase was determined only in one case (see Ref. [P1]).

The Al–Sc–Ti system has also been studied recently; many parallels between Al–Sc–Zr, Al–Sc–Ti and Al–Zr–Ti systems were shown [25–27]. A similar coarsening development of the $L1_2$-structured particles was obtained with the addition of Ti to Al–Sc-based alloys. Ti segregates at the heterophase interface (Al_3Sc particles) and upon ageing at 300 – 450 °C, the $Al_3(Sc,Ti)$ phase exhibits typical “coffee bean” contrast of coherent particles [25]. The principal difference between the Al–Sc–Zr and Al–Sc–Ti alloy comprises a faster diffusion of Zr in Al and a lower maximum solid-solubility of Zr in Al than of Ti in Al [25–27]. Beyond the thermodynamics aspects, the Ti-rich shell should have been created at higher temperatures compared to Zr. The resistivity measurements published by the author of this work (Ref. [P1]) plausibly implicates

that the part of the resistivity decrease if the Al–Sc–Zr system with a small addition of Ti (~ 0.04 wt.%) can be ascribed to the process of the formation of Ti enriched layer. Unfortunately, a particularised research of the microstructure (by APT and/or HR-TEM) of Al–Sc–Zr–Ti-based system has not been published yet.

It was also observed by the author and co-authors that the Al–Sc–Zr system does not prevent but influences natural ageing in solution-treated commercial Al hardenable alloys [P5], e.g. the higher initial hardness of the solution-treated AA6082-ScZr alloy was caused mainly by the presence of the $Al_3(Sc,Zr)$ particles, the microhardness increase during natural ageing in the solution-treated AA6082-ScZr alloy was observed to be slower than the one in the solution-treated AA6082 alloy [P5].

This part of the presented work includes five original author's papers. See followed publications (Refs. [P1–P5]) at the end of the habilitation thesis (*Attached publications*):

[P1] Vlach M., Stulíková I., Smola B., Žaludová N., Černá J.: *Phase transformations in isochronally annealed mould-cast and cold-rolled Al-Sc-Zr-based alloy*, JOURNAL OF ALLOYS AND COMPOUNDS 492 (2010) 1-2, p. 143.

[P2] Vlach M., Cizek J., Melikhova O. et al.: *Early Stages of Precipitation Process in Al-(Mn-)Sc-Zr Alloy Characterized by Positron Annihilation*, METALLURGICAL AND MATERIALS TRANSACTIONS A-PHYSICAL METALLURGY AND MATERIALS 46A (2015) 4, p. 1556.

[P3] Vlach M., Stulikova I., Smola B. et al.: *Phase Transformations and Recrystallization in Cold-Rolled Al-Mn, Al-Sc-Zr and Al-Mn-Sc-Zr Alloy*, ADVANCED DIFFUSION PROCESSES AND PHENOMENA (eds.: Ochsner A., Murch G., Belova I.), DEFECT AND DIFFUSION FORUM 354 (2014), p. 93.

[P4] Vlach M., Stulikova I., Smola B. et al.: *Phase transformations in non-isothermally annealed as-cast and cold-rolled AlMnScZr alloys*, INTERNATIONAL JOURNAL OF MATERIALS RESEARCH 103 (2012) 7, p. 814.

[P5] Vlach M., Smola B., Stulíková I., Očenášek V.: *Microstructure and mechanical properties of AA6082 aluminium alloy with small additions of Sc and Zr*, INTERNATIONAL JOURNAL OF MATERIALS RESEARCH 100 (2009) 3, p. 420.

II. Quaternary Al–Mn–Sc–Zr system

Most Al-based alloys contain transition metals (TM) as alloying additions, but the TM content is limited and does not overcome a fraction of one wt. percent due to the very low solubility [4, 6]. TM elements such as manganese (Mn) form dispersoids in the Al-based alloys and they are extensively used in order to control the microstructure during heat exposure to prevent recrystallization [6, 28].

Al–Mn alloys belong to a group of non-hardenable Al-based alloys featuring brilliant workability, corrosion resistance and weldability [6]; the alloys have become the favourite for a wide range of applications, e.g. can stock, building and construction, fins of automotive heat exchangers [29–31]. Although the Al–Mn alloys exhibit high structure stability under a long-term heating, they demonstrate poor strength properties [6]. On the Al-rich side, Mn and Al form an eutectic phase diagram with the invariant equilibrium temperature of ~ 665 °C and main phase in diluted Al–Mn alloys – Al_6Mn phase – has an orthorhombic lattice [6].

Precipitation of these particles influences the resistivity significantly, but it has a negligible effect on hardness [P3]. The diffusion calculations have shown that Mn-containing dispersoids in the as-cast alloys do not form at temperatures lower than ~ 300 °C during a heat treatment [27, 32].

Despite a number of investigations of the Al_3Sc and/or $Al_3(Zr,Sc)$ phase, only poor data in basic research literature are systematized about Al–Mn-based alloys with Sc and/or Zr. There were only a few works of the others, mainly from last years (e.g. Refs. [6, 10, 29, 32–35]). The solubility of Mn in Al_3Sc phase and of Sc and Zr in Al_6Mn was observed as negligible [6]. Mn has no virtually effect on the solubility of scandium, while Sc and Zr essentially decrease the solubility of Mn in solid Al [6, 10, 29]. The author of this work and co-authors studied the effect of Mn addition on microstructure and mechanical properties of the as-cast and heat-treated Al–Sc–Zr-based alloys with a various content of Mn and Zr – see Refs. [P2–P4, P6]. Relative resistivity changes and the microhardness of the as-cast and heat-treated Al–Mn–Sc–Zr alloys exhibit a very similar dependence on annealing temperature. Precipitation of the Al_3Sc particles and subsequent Zr-segregation to the Al_3Sc/α-Al matrix interfaces were responsible for the main resistivity decrease and the peak microhardness in all these alloys. The same situation was already observed in the ternary Al–Sc–Zr system (see above). The microhardness decrease was observed slightly delayed during the annealing in the alloys with the higher Zr content due to a higher oversaturation of Zr. No influence of the presence of Mn on precipitation processes of the Sc,Zr-containing particles up to 450 °C was detected. The massive precipitation of the Mn-containing particles was observed only at temperatures higher than ~ 510 °C in the as-cast Al–Mn–Sc–Zr alloys. We also applied a specific high temperature heat treatment which was performed at 610 °C for 18 hours with several steps of slow heating rates to provide a depletion of Mn in solid solution during this treatment [P6]. Presence of the overaged $Al_3(Sc,Zr)$ particles and rodlike particles of the Al–Mn system after the annealing was proved. But no effect of the Mn content (except different size of the Al_6Mn particles) on microstructure, resistivity and hardness values was observed.

The apparent activation energy for precipitation of the Al_3Sc particles in the as-cast Al–Mn–Sc–Zr alloys was determined as (116 ± 9) $kJ \cdot mol^{-1}$. It agrees with the apparent activation energy for precipitation of the Al_3Sc phase determined in the binary Al–Sc alloys [36, 37] and in the ternary Al–Sc–Zr alloys (see above). No other thermal response in the as-cast Al–Mn–Sc–Zr alloys was observed.

From the results obtained in the as-cast Al–Mn–Sc–Zr alloys it can be concluded that the decomposition sequence of the supersaturated solid solution of the as-cast Al–Mn–Sc–Zr alloys is compatible with the decomposition sequence of the Al–Sc–Zr system and also with the formation of Mn(,Fe)-containing particles. It can probably be also highly determined that the addition of Mn does not influence the decomposition of solid solution of the ternary Al–Sc–Zr system.

We also attempt to enlarge the knowledge about the early precipitation stages in the as-cast Al–Mn–Sc–Zr alloys during non-isothermal annealing by positron annihilation spectroscopy (PAS) enabling to investigate clustering of solute atoms at the atomic scale (see Ref. [P2]). This technique has never been used in the Al–Mn-, Al–Sc- and/or Al–Zr-based alloys so far. It was recently shown that positrons trapped at defects are preferentially annihilated by Sc electrons.

The result of the PAS observation testified to significantly enhanced concentration of Sc in the vicinity of dislocations indicates that Sc atoms segregate at dislocations – dislocations are probably surrounded by solute Sc-atoms (in the as-cast state). The diffusivity of Sc solutes was enhanced by quenched-in vacancies and also by segregation of Sc at dislocations which shifted the onset of Sc clustering already to ~ 150 °C. A rise of the contribution of trapped positrons annihilated by Zr electrons starting at ~ 240 °C and attaining maximum at ~ 300 °C confirms that Zr electrons are incorporated into Sc-rich particles already at these temperatures. Mn solutes were not involved in the precipitation processes up to ~ 400 °C as the contribution of trapped positrons annihilated by Mn electrons was negligible.

a. Effect of cold-rolling on precipitation processes in as-cast Al–(Mn–)Sc–Zr alloy

The effect of particles introduced during heat treatment on recrystallization in the deformed commercial Al–Mn-based alloys has been studied extensively in last period [32, 38–41]. Dispersoids with the content of Mn increase recrystallization temperature and improve weldability in the deformed alloys [6]. However, it was shown that Mn-containing particles larger than ~ 2 μm act as recrystallization grain nucleation sites [20, 38]. It has also recently been observed that cold rolling helps to accelerate precipitation of Mn-containing particles and the recrystallization process with the exception of heavy rolling ($\varepsilon \geq 3.5$) [28, 29, 39]. Mn addition in Al-based alloys is usually accompanied by Fe and Si elements which highly decrease the solubility of Mn in solid Al [6, 34]. Fe and/or Si additions degrade the recrystallization resistance of the Al–Mn alloy with Zr addition [29, 34]. It implicates that the amount of Fe and Si in the commercial Al–Mn-based alloys should be reduced [4]. Although the diffusivity of Mn in Al at temperatures below ~ 400°C is relatively low [27, 32], Mn-containing dispersoids can be formed during a heat treatment in deformed Al–Mn alloys already at temperatures above ~ 350 °C [32, 39, 41].

Comparison of the Al–Mn alloy with and without cold-rolling was done by the author of this work and co-authors in Ref. [P3]. The alloy was studied during step-by-step quasilinear annealing (QA) from 200 °C up to 600 °C with heating rate 100 K/h followed by isothermal annealing at 600 °C/5 h. The pronounced resistivity decrease of the cold-rolled Al–Mn alloy during the annealing corresponded to the massive Al_6Mn-phase precipitation. A microstructure observation of the cold-rolled Al–Mn alloy at the end of the QA showed the presence of the Al_6Mn and/or $Al_6(Mn,Fe)$ particles of a size ~ 800 nm in (sub)grain interiors and of ~ 10 μm at grain boundaries respectively. On the other hand, a continuous microhardness decrease was observed in the cold-rolled Al–Mn alloy during the annealing. The initial difference in microhardness introduced by cold rolling almost disappears due to recovery and recrystallization after annealing at 500 °C. It could also be seen that the precipitation of the Mn-containing particles has an insignificant effect on hardness.

Comparison of the ternary Al–Sc–Zr alloys with and without cold-rolling was done by the author and co-authors in Refs. [P1, P3]. It is well known that deformed structure (dislocations) and subgrain boundaries introduced by cold-rolling can facilitate solute diffusion. The diffusivity calculations and experiments show that a reasonable long-range Sc-diffusion in the cast Al–based alloys is activated already above ~ 210 °C [P1, P2, 6, 12, 13, 42, 43]. The diffusivity of Sc-

solutes can be also enhanced by a large amount of quenched-in vacancies and by segregation of Sc at dislocations which shifted the onset of Sc clustering already to ~ 160 °C (Ref. [P2]). The relatively fast diffusing Sc-atoms only precipitate as coherent clusters and/or very small dispersoids with fcc ($L1_2$) structure [P2, 13, 42, 43]. These pre-existing dispersoids then act as nucleation sites for the additional precipitation of the Al_3Sc and/or $Al_3(Sc,Zr)$ precipitates. The decomposition of the solid solution in the Al–Sc–Zr alloys up to ~ 300 °C was observed slightly enhanced in the cold-rolled alloy (see Refs. [P1, P3]), e.g. nucleation and growth of the Al_3Sc phase due to the easier diffusion consequently probably start in (sub)grain boundaries and their vicinity at lower annealing temperatures (Δt ~ 20 °C). However, the direct microstructure observation in cold-rolled alloys up to ~ 300 °C was not done as the TEM at even not-deformed alloys gave only a weak evidence of Al_3Sc particles at this range of the annealing temperatures. Subsequent annealing leads to simultaneous coarsening and partial dissolution of the $Al_3(Sc,Zr)$ phase in the Al–Sc–Zr alloy. It agrees well with the microhardness decrease in both types of the alloys. The microhardness of the cold-rolled alloys at temperatures above ~ 500 °C was very close to the values of the as-cast alloys. It can not only be connected with faster coarsening of the $L1_2$-structured particles but also with substructure recovery and recrystallization in the cold-rolled alloy. And it also seems to be very probable that at higher annealing temperatures (above ~ 330 °C) precipitation of the Sc,Zr-containing particles is mainly controlled by bulk diffusion of Sc atoms. This conclusion agrees with the obtained results in an Al-0.25wt.%Sc alloy where the precipitation and growth kinetics of the Al_3Sc particles were found to be unaffected by the presence of a deformation substructure [4]. No effect of cold-rolling on the Al_3Sc particles precipitation was also observed in ternary Al–Sc–Zr alloys [P1]. It is good noticing that no recrystallization at 400 °C/16 h was observed in the cold-rolled alloys. A partial recrystallization of the alloys was clearly registered after annealing at 550°C/60 min, the coarsened grain structure (5–15 μm) was observed. Electron backscatter diffraction (EBSD) analysis of cold-rolled Al–Sc–Zr alloy at 550°C/16 h revealed recrystallized grains (~ 20 μm) which are developed in originally large grains, previously deformed and afterwards recovered. These results are in a great agreement with observation of the other authors on the Al–Sc–Zr alloys with a comparable Sc and Zr content where the first evidence of partial recrystallization was observed at 540 °C after annealing time for 60 min [6].

While both experimental and theoretical analyses of recrystallization in binary Al-based alloys have received attention in recent years [38, 44–47] and nucleation and precipitation kinetics of the Al_3Sc phase in undeformed aluminium have recently been documented [6, 10, 13], detailed studies of microstructural evolution and recrystallization in the presence of the additional very fine precipitates with the $L1_2$ structure due to addition of Sc and Zr in deformed Al–Mn-based alloys are far from clear. Many industrial Al-based alloys contain a mixed particle structure of coarse large inclusion due to casting and fine particles introduced during heat treatments. Some models for a recrystallization reaction, recovery kinetics and microstructural evolution in the presence of fine precipitates in the Al alloys were constructed and subjected to experimental analysis – e.g. Refs. [32, 38, 44–47]. However, the complexity of this situation due to the processing such as cold-rolling, extrusion etc. which are plentifully used in industry makes detailed descriptions of this process complicated. That was the reason why a comparison of the quaternary Al–Mn–Sc–Zr alloys with and without cold-rolling was done by the author and co-

authors in Refs. [P3, P7], the differently cold-rolled Al–Mn–Sc–Zr materials were investigated with respect to characterization of phase transformations and to determination of the structure.

In the Al–Mn–Sc–Zr alloys (see Ref. [P7]) it was observed from the resistivity and differencial scanning calorimetry measurements up to ~ 300 °C that the as-cast alloy and the same alloy after cold-rolling exhibit close similarities – the rolling has no substantial effect on the Al_3Sc-phase precipitation and the decomposition of the solid solution of the Al–Sc–Zr system was observed only slightly enhanced in the cold-rolled Al–Mn–Sc–Zr alloy. Although deformed structures can facilitate solute diffusion and the diffusivity of Sc solutes can be enhanced by segregation of Sc at dislocations (as we observed in as-cast Al–Mn–Sc–Zr alloys – Ref. [P2]), it seems very probable that the coarsening of Sc-containing particles (above ~ 300 °C) in the studied cold-rolled Al–Mn–Sc–Zr alloys is controlled mainly by volume diffusion. This conclusion may be explained by relatively low density of dislocations in (sub)grain interiors in the cold-rolled alloys. On the other hand, the nucleation and growth of the incoherent $Al_6(Mn,Fe)$ phase was significantly enhanced by the deformation structure. This precipitation depends on a deformation degree – the higher deformation the more intensive precipitation of the Mn-containing particles. These results are consistent with results in the deformed Al–Mn-based alloys where the resistivity decrease was more intensive in the deformed specimens and where the deformation strain helped to accelerate the Al_6Mn-phase precipitation (e.g. Ref. [39]). It was also observed that hardening in the cold-rolled Al–Mn–Sc–Zr alloys is mainly caused by precipitation of the particles from the Al–Sc–Zr system. Nevertheless, the massive precipitation Mn-containing particles have a negligible effect on hardness.

The value of the apparent activation energy for precipitation of the Al_3Sc particles ((116 ± 9) kJ·mol^{-1}) in the alloys was observed independently of Mn-content as well as cold-rolling [P7]. The apparent activation energy for the precipitation of the Al_6Mn particles was calculated as (162 ± 22) kJ·mol^{-1} [P7]. The value is slightly higher than the value Q = 140 kJ·mol^{-1} of the Al_6Mn phase precipitation in the Al-2.9wt.%Mn alloy [48]. However, it corresponds to the apparent activation energy Q = 149 kJ·mol^{-1} for the $Al_6(Mn,Fe)$-phase precipitation in the AlMnFeSiCu (AA3000) alloy [49] within the obtained accuracy. No other thermal response was observed in the cold-rolled Al–Mn–Sc–Zr alloys.

No recrystallization was observed in the cold-rolled Al–Mn–Sc–Zr alloys isothermally annealed at 550 °C/8 hours [P3, P7]. The initial microhardness decrease of the Al–Mn–Sc–Zr alloy during the annealing at 550 °C was mainly connected with the recovery effects and/or with a coarsening of the Al_3Sc and/or $Al_3(Sc,Zr)$-phase particles. Although no fast softening in the narrow interval typical for recrystallization processes was detected, the first signs of the recrystallization were found at 550 °C/12 hours. A large improvement of recrystallization resistance in the cold-rolled Al–Mn–Sc–Zr alloy in comparison with the Al–Sc–Zr alloy is evident. Thus, the combination of Mn, Sc and Zr and the presence of the Sc,Zr- and Mn-containing particles have a significant anti-recrystallization effect.

b. Effect of cold-rolling on precipitation processes in Al–(Mn–)Sc–Zr alloys prepared by powder metallurgy

Only few publications dealing with precipitation processing and mechanical properties of powder metallurgy prepared (PM) Al-based alloys with Sc and Zr additions were found, e.g.

Al-based alloy and Al–Mg-based alloy respectively (e.g. Refs. [14, 50]). PM production of the Al–Mn-based alloys with Sc,Zr-content can add other improvements connected with substantial grain refinement and a smaller starting powder size can result in a larger volume fraction of fine Al_3(Sc,Zr) particles [14, 51]. An excellent thermal stability and coherency of the Al_3(Sc,Zr) particles up to annealing temperatures higher than ~ 350 °C as well as the published observation of dislocations pinned by these particles in an Al–Sc–Zr alloy prepared by powder metallurgy [52] and tensile tested at 350 °C attest to postponed dislocation recovery process due to the Al_3(Sc,Zr) particles. No such studies of Al–Mn–Sc–Zr-based alloys prepared by powder metallurgy (PM) have been performed. Thus the author of this work and co-authors have recently published the investigate of the effect of cold rolling on phase transformations and recrystallization behaviour of the Al–Sc–Zr and Al–Mn–Sc–Zr alloys prepared by powder metallurgy – see Ref. [P8].

The Al–Sc–Zr and Al–Mn–Sc–Zr alloys were produced by atomising in argon with ~ 1% of oxygen. The powder was consolidated by extrusion at 350 °C with reduction of 70:18. The part of the extruded alloys was also further deformed by cold-rolling. Microstructure observation revealed similar microstructure in the all alloys with and without cold-rolling. A fine (sub)grain structure (< 1 μm) was developed. TEM proved a fine dispersion of the Al_3(Sc,Zr) particles which precipitated in both alloys in grain interiors during preparation process. Examination of the cold-rolled PM alloys reveals a typical fibrous structure. Hardness values attained an indistinct maximum during the isochronal annealing (30 °C/30 min) at ~ 300 °C due to a slight additional precipitation of the Sc,Zr-containing particles. A slight faster coarsening of the Sc-containing particles was observed in the cold-rolled PM alloys. But the precipitation of the Mn-containing particles was highly enhanced by cold-rolling. Precipitation of the Al_6Mn particles was shifted more than ~ 50 °C to lower temperatures in comparison with PM alloy without cold-rolling, more than ~ 100 °C in comparison to the as-cast Al–Mn–Sc–Zr alloys with subsequent cold-rolling and more than ~ 150 °C in comparison to the as-cast Al–Mn–Sc–Zr alloys. Kinetics of the Al_3Sc precipitation after cold-rolling is comparable for the PM alloys independently of Mn-addition.

The apparent activation energy of the Al_3Sc-phase formation in the cold-rolled PM alloys was calculated as (110 ± 11) kJ·mol^{-1} [P8]. The same independence of this kinetics on Mn-addition can be seen in the non-rolled alloys and the Al–Mn–Sc–Zr powder [P8]. The apparent activation energy of the Al_3Sc-phase formation in the non-rolled PM alloys was calculated as (107 ± 10) kJ·mol^{-1} [P8]. The value of the apparent activation energy for the Al_6Mn-phase precipitation was determined as (144 ± 16) kJ·mol^{-1} in the cold-rolled Al–Mn–Sc–Zr alloy and (152 ± 33) kJ·mol^{-1} in the Al–Mn–Sc–Zr alloy [P8]. It seems to be probable that the values in the PM alloys are affected by deformed structure and (sub)grain boundaries introduced by cold-rolling. However, they agree, within experimental scatter, with the apparent activation energy Q for precipitation of the Al_6Mn phase in as-cast Al–Mn–Sc–Zr alloy after cold-rolling ((162 ± 22) kJ·mol^{-1}) [P7].

EBSD analysis of the Al–Sc–Zr alloy prepared by PM revealed partially recrystallized grains after isochronal annealing (at 570 °C) [P8]. No recrystallization of the Al–Mn–Sc–Zr alloy at this temperature was observed. The texture development of the Al–Sc–Zr alloy prepared by PM seems to be affected by high solid solution strengthening by Mn, see Ref. [P8]. Hardness of the cold-rolled PM alloys decreases during isothermal annealing at 400 °C somewhat faster than

microhardness of the alloys without cold-rolling due to the recovery effects and/or a slightly faster coarsening of the Al_3Sc particles. A partial recrystallization of the cold-rolled Al–Sc–Zr alloys prepared by PM was clearly registered after annealing at 550 °C/1 h. Fully recrystallized structure of the cold-rolled Al–Sc–Zr alloy prepared by PM was observed after 550 °C/16 h. No occurrence of recrystallization was observed after annealing at 550 °C/32 h in the cold-rolled Al–Mn–Sc–Zr alloy prepared by powder metallurgy. A large improvement of recrystallization resistance due to a combination of Mn, Sc and Zr is evident and the presence of the Mn-containing particles at (sub)grain boundaries has a significant antirecrystallization effect.

c. Effect of hot-deformation on precipitation processes in Al–(Mn–)Sc–Zr alloy

The effect of the Mn-, Sc- and Zr-content on recrystallization in binary hot-deformed aluminium alloys has been partially documented [5, 7, 29, 34, 39]. Even much less articles dealing with properties of the hot-deformed Al–Mn–Sc–Zr alloys were published, e.g. Refs. [10, 14, 52–54]. An understanding of the complex interactions between concurrent precipitation and recrystallization in the Al–Mn-based alloys requires further investigation [55, 56].

The author of this work and co-authors recently published investigation of the effect of hot-extrusion (HE) and hot-rolling (HR) on phase transformations and recrystallization behaviour of the Al–Mn–Sc–Zr alloys – see Ref. [P9]. The hot-extrusion of the cast alloy was performed at 350 °C in one step with a reduction 70:18. The hot-rolling of the cast alloy was performed at 300 °C in two steps with a total reduction of 90 %. The alloys were characterized by a dispersion of fine $Al_3(Sc,Zr)$ particles and a fine (sub)grain structure (~ 1 μm) in the direction perpendicular to the deformation. Resistivity measurements during isochronal annealing (30 °C/30 min) indicated a summation of two precipitation stages of the Mn-containing particles (one stage at ~ 340 °C followed by another stage at ~ 410 °C) in both alloys [P9]. Thus the special TEM tilt holder for in-situ heating procedure was performed. Linear annealing from room temperature was done in the same effective rate as the isochronal annealing. Indeed, TEM observed the beginning of the Al_6Mn particles precipitation at (sub)grain boundaries starting at ~ 320 °C. The disappearance of dislocations at ~ 320 °C was observed additionally. First Mn-rich particles inside (sub)grains were observed after annealing up to 400 °C. No recrystallization was observed after isochronal annealing (600 °C) in the both alloys, anyway. The similar development of the Mn-containing particles was observed in the Al–Mn–Sc–Zr alloy prepared by powder metallurgy after extrusion at 350 °C (see above and/or Ref. [P8]) where Mn-containing particles of a size ~ 50 nm in (sub)grain interiors and hundreds of nanometres at (sub)grain boundaries after the isochronal annealing up to ~ 450 °C were observed in the PM alloy. Therefore one can suggest that the two-stage development of the Al_6Mn phase in hot-deformed Al–Mn–Sc–Zr alloys seems to be justified generally. The conclusion can be probably valid also in the cold-rolled Al–Mn–Sc–Zr alloys [P4, P7, P8].

A single exothermic peak corresponding to the Al_6Mn precipitation inside (sub)grain interior was observed on DSC annealing curves of the HE alloy. Two thermal peaks were observed (corresponding to the Al_3Sc-phase precipitation and the Al_6Mn precipitation inside (sub)grains) in the HR alloy [P9].

The HR and HE alloys were also isothermally annealed at 400 and 550 °C. Hardness development was observed similar to each other. It decreases at 550 °C somewhat faster than hardness at 400 °C. Only a partial sporadic recrystallization of the alloys was registered at 550 °C/32 h. Hardness decrease was mainly caused by coarsening of the Sc,Zr-containing particles. The (sub)grain structure was developed from ~ 1 μm at the beginning to ~ 2 μm at 550 °C/32 h. The purpose of Sc and Zr added to the Al–Mn-based alloys may be either to stabilise the microstructure of wrought semi-products (extrusions, rolled plates, forgings etc.) or to provide extra strength to the alloy through precipitation hardening [5, 10]. Hot deformation of Mn, Sc and Zr containing Al alloys can add other improvements connected with substantial grain refinement and/or can increase stability to elevated temperatures over long periods of time [P8, P9, 57].

This part of the presented work includes eight original author's papers. See followed publications (Refs. [P1–P4, P6–P9]) at the end of the habilitation thesis (*Attached publications*):

[P1] Vlach M., Stulíková I., Smola B., Žaludová N., Černá J.: *Phase transformations in isochronally annealed mould-cast and cold-rolled Al-Sc-Zr-based alloy*, JOURNAL OF ALLOYS AND COMPOUNDS 492 (2010) 1-2, p. 143.

[P2] Vlach M., Cizek J., Melikhova O. et al.: *Early Stages of Precipitation Process in Al-(Mn-)Sc-Zr Alloy Characterized by Positron Annihilation*, METALLURGICAL AND MATERIALS TRANSACTIONS A-PHYSICAL METALLURGY AND MATERIALS 46A (2015) 4, p. 1556.

[P3] Vlach M., Stulikova I., Smola B. et al.: *Phase Transformations and Recrystallization in Cold-Rolled Al-Mn, Al-Sc-Zr and Al-Mn-Sc-Zr Alloy*, ADVANCED DIFFUSION PROCESSES AND PHENOMENA (eds.: Ochsner A., Murch G., Belova I.), DEFECT AND DIFFUSION FORUM 354 (2014), p. 93.

[P4] Vlach M., Stulikova I., Smola B. et al.: *Phase transformations in non-isothermally annealed as-cast and cold-rolled AlMnScZr alloys*, INTERNATIONAL JOURNAL OF MATERIALS RESEARCH 103 (2012) 7, p. 814.

[P6] Vlach M., Stulíková I., Smola B., Žaludová N.: *Characterization of phase development in non-isothermally annealed mould-cast and heat-treated Al-Mn-Sc-Zr alloys*, MATERIALS CHARACTERIZATION 61 (2010) 12, p. 1400.

[P7] Vlach M., Stulikova I., Smola B. et al: *Effect of cold rolling on precipitation processes in Al-Mn-Sc-Zr alloy*, MATERIALS SCIENCE AND ENGINEERING A-STRUCTURAL MATERIALS PROPERTIES MICROSTRUCTURE AND PROCESSING 548 (2012), p. 27.

[P8] Vlach M., Stulikova I., Smola B. et al.: *Precipitation in cold-rolled Al-Sc-Zr and Al-Mn-Sc-Zr alloys prepared by powder metallurgy*, MATERIALS CHARACTERIZATION 86 (2013), p. 59.

[P9] Vlach M., Stulikova I., Smola B. et al.: *Annealing effects in hot-deformed Al-Mn-Sc-Zr alloys*, KOVOVE MATERIALY-METALLIC MATERIALS 53 (2015) 5, p. 295.

Role of the Tb and Nd addition in Mg-based alloys

Low density Mg-based alloys allows for a significant weight reduction which raises the effectiveness in a broad range of applications (transport, IT, or leisure industries) [58–61]. Unfortunately, the use of most Mg-based alloys is limited to low temperatures due to a degradation of their mechanical properties above ~ 200 °C. There are several approaches how to overcome the difficulties/obstacles. Particularly promising way is a use of non-traditional alloying elements [58–60] such as rare earth (RE) elements (inclusive Sc and Y) which led to the development of successful commercial WE alloy containing Y and Nd [61–63] and promising high performance alloys containing Sc and Mn in combination with Gd, Y, and Y + Nd [59, 63–65]. Mostly relative thermally stable precipitates of transient phases are responsible for peak hardening, improved creep properties and good thermal stability in Mg–RE-based alloys [61–65]. These alloys containing RE have also recently been intensively investigated as a biodegradable material suitable for degradable orthopaedic implants and/or degradable stents [66–69]. Biodegradable alloys based on Mg recently receive a lot of public attention due to requests for implants that do not need removing after a healing process. Such implants improving quality of life of the individual highly demand proper mechanical properties, biocompatibility, and optimal corrosion in body fluids [66–70].

Three basic types of sequential precipitation are known in Mg–RE-based supersaturated solid solutions [59, 61, 71, 72]:

a) Mg–Y type (Y, Tb, Dy, Ho, Er, Tm, Lu)
   α' (hcp) $\rightarrow$ β'' ($D0_{19}$) $\rightarrow$ β' (cbco) $\rightarrow$ β ($Mg_{24}Y_5$, bcc);
b) Mg–Nd type (Ce, Nd)
   α' (hcp) $\rightarrow$ GP zones $\rightarrow$ β'' ($D0_{19}$) $\rightarrow$ β' (orthorhombic) $\rightarrow$ β_1 (fcc) $\rightarrow$ β ($Mg_{12}Nd$, bct) $\rightarrow$ β_e ($Mg_{41}Nd_5$, bct);
c) Mg–Gd type
   α' (hcp) $\rightarrow$ β'' ($D0_{19}$) $\rightarrow$ β' (cbco) $\rightarrow$ β_1 (fcc) $\rightarrow$ β (Mg_5Gd, fcc).

The β'' ($D0_{19}$) transient phase has hexagonal structure ($a = 2 \cdot a_{Mg}$, $c = c_{Mg}$) and it is coherent in the hexagonal close packed (hcp) Mg matrix. The β' phase (cbco – c-based centred orthorhombic, $a = 2 \cdot a_{Mg}$, $b = 8 \cdot d(1\text{-}100)_{Mg}$, $c = c_{Mg}$) is a transient phase semi-coherent with the Mg matrix. The transient β' phase following the DO_{19} phase in the Mg–Nd type sequence has an orthorhombic structure ($a = 2 \cdot a_{Mg}$, $b = 4 \cdot d(1\text{-}100)_{Mg}$, $c = c_{Mg}$) and the precipitation sequence ends with an equilibrium base centred tetragonal phase (a = 1.47 nm, c = 1.04 nm). It was earlier believed that the stable phase in the Mg–Nd system has the same structure with lattice parameters a = 1.03 nm, c = 0.59 nm and composition of the $Mg_{12}Nd$ phase.

It is good to notice when the Mg–Y and Mg–Nd groups are combined in magnesium alloys, Mg–Gd decomposition sequence is usually observed, e.g. in WE-based alloys (Mg–Y–Nd-based alloys) or in Mg–Dy–Nd and Mg–Gd–Nd alloys [59, 60, 71–77]. The transient β_1 (a = 0.74 nm, $d(220) \sim d(0002)_{Mg}$) phase appears in the precipitation sequences. It has more recently been found in WE-based alloys and also in Mg–Tb–Nd alloy [71–74]. Modification of the precipitation sequence and phase morphology depends on product technology and thermomechanical treatment [71–77]. Not only the volume fraction but also the arrangement, the orientation relationship and aspect ratio of the precipitates affect the mechanical and creep properties [71, 72, 78].

Precipitates of transient phases are usually the most important in age hardening of Mg–RE-based alloys as distributions of finer plates in a higher number density than for the equilibrium phase can be developed. Unfortunately, thermodynamic assessment is predominantly available for equilibrium phases of the Mg–RE systems only and only little information can be found about activation energy of transient phase's precipitation in Mg–RE-based alloys, e.g. Refs. [76, 79, 80].

Hexagonal structure of Mg and its alloys results in low ductility and easy failure of parts with a complex geometry. Despite the favourable strength and thermal stability, a disadvantage of several Mg–based alloys consists in a poor ductility insufficient for most of potential industrial applications. Grain refinement is a well-known method how to improve ductility of metallic materials. Materials prepared by powder metallurgy route (PM) carry a smaller grain size and a fine distribution of secondary phases which improve mechanical strength and increase corrosion resistance [81]. PM proceeds usually by rapid solidification of melt droplets atomized in a gas flow. As a non-equilibrium process it may extend solid solubility of solutes or lead to formation of non-equilibrium phases [82]. During compaction of powders performed often by hot pressing and/or hot extrusion an undesirable phase development can proceed and influence mechanical properties and their thermal stability. Severe plastic deformation (SPD) applied in an appropriate way enables the achievement of an extreme grain refinement and is capable of producing bulk materials with ultra-fine grained (UFG) structure; see Ref. [83] for a review. A number of techniques based on SPD have been developed so far. However, the strongest grain refinement was achieved by high pressure torsion (HPT) [84]. An extremely small grain size (~ 100 nm) leads to a significant volume fraction of grain boundaries which represent obstacles for movement of dislocations and cause a significant hardening additional to the age hardening effect caused by precipitates. As a consequence, the UFG metals are often characterized by a favourable combination of a very high strength and a reasonable ductility [83]. Then the precipitation effects can be influenced by the concentration of nucleation sites and by the diffusivity of solutes. Dislocations enhance both these parameters. Therefore, a high dislocation density introduced by SPD may influence the precipitation processes. Interestingly, because both the PM and the UFG structure deformed Mg-alloys exhibit not only higher hardness but also enhanced ductility compared with the coarse grained alloys [85]. Obviously this is very important for improving the workability of age-hardenable Mg-alloys which is still not satisfactory.

I. Binary Mg–Tb system

Binary Mg–Tb alloys are the base for novel creep resistant hardenable Mg alloys with RE elements [58]. The maximum solubility of Tb in Mg is ~ 24 wt.% at the eutectic temperature of ~ 559 °C, i.e. relatively large, but it rapidly decreases at lower temperatures, e.g. at ~ 200 °C it becomes about only ~ 9 wt.% [60].

Our preliminary studies involved electrical resistivity investigations of solution treatment of Mg–10wt.%Tb and Mg–15wt.%Tb alloys – see Ref. [P10]. Solution heat treatment of the as-cast alloys was carried out in argon protective atmosphere at 530 °C. A grain size in as-cast alloys was observed dependent on the solute concentration. The contribution of the addition of 1 at.% of Tb to the resistivity of Mg was calculated as 83.6 nΩ·m/at.% (at 77 K) in Ref. [P10]. We conclude from the main result of our preliminary study that the isothermal

annealing at 530 °C for Mg–Tb binary alloys approach the saturated resistivity values for reasonable times showing the possibility to quench in the supersaturated solid solutions.

After the characterization of the initial solution-treated state the samples of the Mg–15wt.%Tb alloy were subjected to step-by-step isochronal annealing [P10–P12]. A significant rise of (micro)hardness (HV) values occurred after annealing above 100 °C and it was accompanied by a strong decrease of electrical resistivity in the temperature range up to ~ 180 °C. This gives clear evidence that precipitation takes place in the samples. Indeed, TEM investigations performed on the samples annealed up to 180 °C revealed precipitation of the transient β'' phase with $D0_{19}$ structure. Although β'' phase is coherent with Mg matrix, in the early stages of precipitation the β'' phase particles contain vacancy-like defects. This is not surprising since the formation of β'' phase particle occurs in thermally activated diffusion of Tb atoms via the vacancy mechanism. Hence, in the early stages of precipitation the structure of the β'' phase particles is far from being perfect and contains vacancies. Similar effect was observed in the early stages of precipitation in Mg–Gd alloys [86]. Further annealing at higher temperatures leads to a decrease in HV due to growth and/or dissolution of the β'' phase particles. After a drop at 260 °C hardness HV values increased with temperature again. It exhibited a local maximum at ~ 280 °C caused by precipitation of the β' phase with cbco structure. Since the β' phase precipitates are semi-coherent with the Mg matrix misfit defects are created. Annealing above 280 °C led to growth and subsequently dissolution of the β' phase precipitates which was accompanied by decreasing of HV. The complete dissolution of the β' phase occurred at ~ 400 °C. At temperatures above ~ 450 °C there was a very slight hardening peak caused by precipitation of the stable β phase.

The formation of the β' and β phases could not be detected by DSC due to low volume fraction of precipitating particles. There was only a slight thermal response to formation of the β'' phase. The apparent activation energy for precipitation of the β' phase particles was determined approx. 97 $kJ \cdot mol^{-1}$. This value is higher than the activation energy of ~ 75 $kJ \cdot mol^{-1}$ determined for Guinier-Preston zone formation in Mg–Nd alloy [79] but agrees well with the activation energy for precipitation of β' phase plates with $D0_{19}$ structure in Mg–Nd–Gd–Zr alloy [80].

a. Ultra-fine grained Mg–Tb alloy

To elucidate the effect of plastic deformation on the precipitation sequence we also studied Mg–13wt.%Tb alloy with ultra-fine grained structure prepared by high pressure torsion (HPT) – see Ref. [P11]. In HPT processing, a disk-shaped sample with diameter of ~ 10 mm located between two anvils is subjected to a compressive pressure of several GPa and simultaneously strained by a rotating anvil. It was observed that the HPT sample exhibits a structure with a mean grain size ~ 100 nm and a high density of dislocations introduced by a severe plastic deformation. TEM and ED also proved the high-angle miss-orientation of neighbouring grain and no precipitates in the as-deformed sample.

The temperature dependence of microhardness in the deformed alloy subjected to isochronal annealing showed the hardening peak due to precipitation of finely dispersed coherent particles the β' phase. We also observed that precipitation of this phase started at lower temperatures (~ 20 °C) than in the solution-treated alloy (see above). This effect is

obviously due to ultra-fine grained structure and high dislocation density in the HPT-deformed alloy. The significant volume fraction of grain boundaries and high dislocation density enhanced the diffusivity of Mg and Tb atoms due to diffusion along grain boundaries or dislocation lines. Moreover, dislocations might serve additional nucleation centres for precipitates.

Above annealing temperature of ~ 220 °C recrystallization took place in the deformed sample leading to a significant softening since deformed UFG matrix with high dislocation density was gradually replaced by coarser dislocation-free recrystallized grains [P11]. The hardening peak caused by precipitation of the β' phase was not observed due to softening by recrystallization occurring simultaneously. Recrystallization in a deformed sample was finished at 360 °C and hardness becomes comparable with that of solution-treated alloy [P10–P12].

b. Natural aging of the solution-treated Mg–Tb alloy

Natural aging (NA) occurring due to clustering of solute atoms and vacancies at ambient temperature after quenching material from high annealing temperature is well known in Al-based alloys, e.g. Refs. [87, 88, P5]. The NA period has a deleterious effect on a subsequent increase in yield stress during artificial ageing in many Al-based alloys [8, 9], while in more dilute alloys the effect of NA can improve the ageing response [P5, 89, 90]. Advanced techniques have recently revealed experimentally the formation of solute clusters in the NA process of Al-based alloys and they enable even to study kinetics and chemistry of clusters and subsequent early precipitation stages, e.g. Refs. [91–93]. Solute clusters formed during NA hinder movement of dislocations and cause significant strengthening of the material. Natural aging is important for industrial processing since the peak hardness attainable at elevated temperature is affected by the period for which the material was stored at room temperature [94]. Contrary to Al-based alloys, the natural ageing of Mg-based alloys is not common. It was only reported for Mg–Zn based alloys [95, 96] where an extremely large incubation period (~ 9 weeks) was observed in hardness response to natural ageing in the binary Mg–7wt.%Zn alloy and in the commercial ZK60 alloy. According to the author's knowledge remarkable natural ageing occurring on the time scale of less than 1 month has recently been observed in binary Mg-alloys with Tb (and Gd respectively) for the first time in Refs. [P12, 97].

Single vacancies in Mg are mobile well below room temperature and in quenched sample quickly disappear by diffusion to sinks at the surface and grain boundaries [98]. However, vacancy-solute pairs are more stable and may remain in the alloys quenched to room temperature. Our investigations (see Refs. [P12, 97]) of the solution-treated Mg–13wt.%Tb revealed that the alloys in the as-quenched state contain vacancies bound to Tb solutes. In the as-quenched state a significant contribution of positrons annihilated in the vicinity of Tb atoms was observed. This contribution came from positrons trapped at quenched-in vacancies associated with Tb solutes [P12, 97]. The development of microhardness during natural aging of the Mg–13wt.%Tb alloy was characterized as HV rise with increasing aging time. The time dependence of HV plotted in the logarithmic time scale exhibits an S-shaped curve typical for natural aging. Contrary to the alloy aged at ambient temperature, alloy stored in liquid nitrogen do not show any increase of HV [P12, 97]. This testified that natural aging occurring in the studied Mg–13wt.%Tb alloy is a thermally activated process. Since the solubility of Tb in Mg strongly decreases with decreasing temperature small clusters of Tb atoms were formed during aging at ambient temperature by diffusion of Tb alloying elements. The driving force for the

clustering of Tb atoms is solute supersaturation in the Mg matrix [P12, 97]. Clustering process is obviously controlled by temperature and is facilitated by quenched-in vacancies bound to solute atoms the quenched-in vacancies facilitate agglomeration of Tb solutes into tiny clusters. The Mg–Tb sample naturally aged for 4 days contained quenched-in vacancies in concentration comparable to those in the quenched sample [P12, 97]. Hence, quenched-in vacancies remaining in the samples facilitate diffusion and clustering of solutes. However, after natural aging for 2 months the solute clusters were fully developed and bound vacancies were removed from the samples [P12]. The reason for this is when the formation of the clusters was finished the vacancies disappeared. The mean size of the Tb-rich solute clusters formed by NA is a few nanometres (nm) only, i.e. they are too small to be visible by transmission electron microscopy. But they can be observed by atom probe tomography (APT). Well-developed nanosized Tb-rich particles most probably representing very early stage of β' phase formation were recently observed by APT in Mg–13wt.%Tb alloy long term aged at ambient temperature for 1.5 year [99].

Solution-treated Mg–Tb alloy aged at ambient temperature for ~ 2 months was investigated during step-by-step isochronal annealing with effective heating rate of 1 K/min [97]. Precipitation of β''-, β'- and β-phase was distinguished in the Mg–Tb alloy. The formation of the β' phase with $D0_{19}$ structure was detected in the temperature range 140 – 200 °C. HV rose due to the formation of these particles and maximum hardening was achieved. It was also observed that quenched-in vacancies bound to solutes were removed by annealing up to ~ 100 °C. Solution-treated Mg–Tb alloy which was isochronally annealed immediately after quenching, i.e. prior to development of Tb clusters, was also investigated – see Ref. [97]. Lower initial HV of this sample was, therefore, caused by the fact that Tb clusters had not been developed yet. Obviously hardening in the sample annealed immediately after quenching was also lower compared to the one in the aged sample. Thus, natural aging had beneficial effect on hardening in the Mg–Tb alloy [P12, 97]. This is probably due to the fact that small Tb clusters formed during natural aging serve as nucleation centres for the β' phase and enable formation of finely dispersed particles.

This part of the presented work includes three original papers. See followed publications (Refs. [P10–P12]) at the end of the habilitation thesis (*Attached publications*):

[P10] Stulíková I., Smola B., Žaludová N., Vlach M., Pelcová J.: *Development of electrical resistivity due to solution treatment of squeeze cast magnesium-rare earth alloys*, KOVOVE MATERIALY-METALLIC MATERIALS 43 (2005) 4, p. 272.

[P11] Melikhova O., Cizek J., Hruska P., Vlcek M., Prochazka I., Vlach M. et al.: *Influence of Deformation on Precipitation Kinetics in Mg-Tb Alloy*, RECENT ADVANCES IN MASS TRANSPORT IN MATERIALS (eds.: Ochsner A., Belova I., Murch G. E), DEFECT AND DIFFUSION FORUM 322 (2012), p. 151.

[P12] Cizek J., Smola B., Stulikova I., Hruska P., Vlach M. et al.: *Natural aging of Mg-Gd and Mg-Tb alloys,* PHYSICA STATUS SOLIDI A-APPLICATIONS AND MATERIALS SCIENCE 209 (2012) 11, p. 2135.

II. Ternary Mg–Tb–Nd system

Mg–Tb–Nd ternary alloy is taken for a novel hardenable alloy with enhanced strength and favourable creep properties even at elevated temperatures. Our preliminary studies involved electrical resistivity investigations of solution treatment of the Mg4Tb2Nd (Mg–3.96wt.%Tb–2.53wt.%) alloy – see Ref. [P10]. Solution heat treatment of the as-cast alloy was carried out in argon protective atmosphere at 500 °C. After the characterization of the initial solution-treated state the alloy was subjected to step-by-step isochronal annealing [P10]. The cast and solution-treated Mg–Tb–Nd alloys with ~ 3.2 – 4.0 wt.% Tb and ~ 1.7 – 2.5 wt.% Nd belong to Mg alloys where all three transient phases (β'', β' and β_1) gradually develop during isochronal annealing and can therefore serve as a model alloy for investigation of an influence of material manufacturing and of treatment history on secondary phases development – see Refs. [P10, P13–P16]. The precipitation sequence of the Mg–Tb–Nd alloy included successively ($D0_{19}$ clusters,) $D0_{19}$ particles, extremely small particles of the β' phase, β_1 phase with fcc structure, β phase of the Mg_5(Tb,Nd) type and β_e phase of the Mg_{41}(Tb,Nd)$_5$ type. All the particles except the first and last ones were observed as plates oriented in the Mg matrix in a triangular arrangement [P14]. The size of the cbco phase was observed extremely small. Only irregular particles of the Mg_{41}(Tb,Nd)$_5$ type phase were rarely found after the successive annealing up to 500 °C. The temperature range of the β_1 phase precipitation hardening corresponds very well to the heat flow and PAS responses caused by this process [P14]. The activation energy obtained from the DSC data analysis using the Kissinger method increased from (92 ± 7) kJ·mol^{-1} to (197 ± 10) kJ·mol^{-1} for the $D0_{19}$ formation to the development of the β_1 phase. The activation energy of both β and β_e phases formation was observed lower than the energy for the β_1 phase formation, (139 ± 29) and 173 kJ·mol^{-1} [P14].

The corrosion behaviour is one of the critical properties in the application of Mg alloys and can be generally improved by the addition of RE. Thus we also studied the corrosion characteristics of the Mg–Tb–Nd alloy – see Ref. [P13]. The Mg–Tb–Nd alloy had a higher corrosion current density and passivity current density than the commercial magnesium WE43 alloy. However, the Mg–Tb–Nd alloy showed a high hydrogen evolution rate initially, which continuously increases with time. This increase indicates that the corrosion products developed on the Mg–Tb–Nd alloy have a non-protective nature.

a. Ultra-fine grained Mg–Tb–Nd alloy

Severe plastic deformation, which is able to fabricate ultra-fine grained structure, could represent a promising way for improvement of properties of Mg-based alloys due to the effects of an extreme grain size reduction [83, 84]. To fabricate the UFG structure, the solution-treated Mg3Tb2Nd (Mg-3.2wt.%Tb-1.8wt.%) alloy was deformed by HPT at room temperature using 5 rotations under a high pressure of 6 GPa. After a detailed characterization of the as-deformed microstructure, the specimen was subjected to step-by-step isochronal annealing – see Ref. [P16]. The as-deformed specimen showed a homogeneous UFG structure with grain size ~ 100 nm. A high density of dislocations was observed by TEM. Dislocations were homogeneously distributed throughout all grains. Electron diffraction pattern testified long angle miss-orientation of neighbouring grains. No precipitates were found in the as-deformed state.

A strong grain refinement and a high dislocation density led to a substantial hardening reflected by an increase of microhardness: the HPT-deformed alloy exhibits ~ 140 % higher microhardness than the solution-treated Mg–Tb–Nd alloy (see above).

The microstructure development during the isochronal annealing of the deformed Mg3Tb2Nd alloy included not only the precipitation effects, but also the recovery of the defects introduced by plastic deformation. The clear evidence for a recovery of dislocations in the temperature range of 100 – 180 °C occurred [P16]. Although the dislocation density decreased, no grain growth was detected by TEM up to ~ 200 °C. It means that the ultra-fined grained Mg3Tb2Nd alloy exhibited relatively high thermal stability of UFG structure which is favourable for further applications.

Precipitation of β'' phase occurred at similar temperatures as in the solution-treated Mg–Tb–Nd alloy [P14, P16]. The β_1 phase observed by TEM after annealing up to 240 °C was also reflected by an increase of microhardness. Thus the main difference between HPT-deformed and coarse grained (solution-treated) alloy consists in the fact that the precipitation of β_1 phase starts in the UFG alloy already at lower temperatures (Δt ~ 80 °C). It has two reasons: (i) an extremely small grain size leads to a significant volume fraction of grain boundaries. Defects at grain boundaries serve as nucleation centres for the second phase particles. (ii) Diffusivity of Tb and Nd atoms is enhanced by a possibility to diffuse along grain boundaries. Both these factors facilitate precipitation effects in the UFG alloy and shift precipitation of β_1 phase to lower temperatures [P14, P16].

b. Mg–Tb–Nd alloy prepared by powder metallurgy

To elucidate the effect of the preparation by PM on the precipitation sequence we also studied Mg4Tb2Nd (Mg-3.6wt.%Tb-2.3wt.%) alloy prepared by powder metallurgy (PM) route (powder cold pressing and extrusion at 280 °C) – see recently published Ref. [P15].

The initial structure of the PM alloy was partly recovered or recrystallized with (sub)grains size not exceeding ~ 5 μm. HV value of the PM alloy in the initial state was higher than the hardness of the solution-treated alloy even though the concentration of solute atoms in the matrix is lower in the PM alloy [P14–P16]. It resulted from fine grain structure of the PM alloy. Hardening due to isochronal annealing is negligible in the PM alloy contrary to the solution-treated alloy, as contributions of structure and precipitation effects to hardness did not add linearly and volume fraction of precipitated phases was not the same in these materials due to a different supersaturation. Precipitation of transient phases in a sequence $\beta'' \rightarrow \beta' \rightarrow \beta_1 \rightarrow \beta \rightarrow \beta_e$ was identified in the PM alloy in course of the isochronal annealing (30 °C/30 min) [P15]. The first precipitation stage of the $D0_{19}$ clusters known from the solution-treated alloy as well as precipitation of equilibrium β_e phase resulted in negligible effects either in resistivity or in differential scanning calorimetry of the PM alloy. It was observed that powder metallurgy way of alloy preparation changes neither the precipitation sequence in the Mg4Tb2Nd alloy nor activation energy values of the particular precipitation processes but shifts temperature ranges of these processes. Cuboidal particles (most probably hydrides of RE and of Mg) developed during the alloy production remained even after isochronal annealing up to 510 °C.

This part of the presented work includes five original papers. See followed publications (Refs. [P10, P13–P16]) at the end of the habilitation thesis (*Attached publications*):

[P10] Stulíková I., Smola B., Žaludová N., Vlach M., Pelcová J.: *Development of electrical resistivity due to solution treatment of squeeze cast magnesium-rare earth alloys*, KOVOVE MATERIALY-METALLIC MATERIALS 43 (2005) 4, p. 272.

[P13] Neubert V., Stulíková I., Smola B., Mordike B. L., Vlach M., Bakkar A., Pelcová J.: *Thermal stability and corrosion behaviour of Mg–Y–Nd and Mg–Tb–Nd alloys*, MATERIALS SCIENCE AND ENGINEERING A-STRUCTURAL MATERIALS PROPERTIES MICROSTRUCTURE AND PROCESSING 462 (2007) 1–2, p. 329.

[P14] Smola B., Stulikova I., Cerna J., Cizek J., Vlach M.: *Phase transformations in MgTbNd alloy*, PHYSICA STATUS SOLIDI A-APPLICATIONS AND MATERIALS SCIENCE 208 (2011) 12, p. 2741.

[P15] Stulikova I., Smola B., Vlach M., Kudrnova H., Piesova J.: *Influence of powder metallurgy route on precipitation processes in MgTbNd alloy*, MATERIALS CHARACTERIZATION 112 (2016), p. 149.

[P16] Čížek J., Procházka I., Smola B., Stulíková I., Vlach M. et al.: *Precipitation effects in ultra-fine-grained Mg-RE alloys*, INTERNATIONAL JOURNAL OF MATERIALS RESEARCH 100 (2009) 6, p. 780.

Role of the H-induced defects in the selected Pd films

Hydrogen (H) absorption and hydride formation in metals are a great field of interest due to their use for hydrogen storage in bulk materials and for sensor applications in thin metal films [100]. It is known that hydrogen strongly interacts with open volume defects (vacancies, dislocations etc.) in a host metal lattice [101]. It was shown that H is not only trapped at existing defects, but also a high amount of new defects can be created by H-loading [102, 103]. Hydrogen trapping in defects also reduces hydrogen diffusivity in materials [100, 104].

Hydrogen dissolved in interstitial sites in a host metal lattice can cause remarkable volume expansion [105]. Bulk sample loaded with hydrogen expands in all directions and the lattice expansion increases with increasing hydrogen concentration up to a phase transition into a hydride phase. Despite the number of investigations of the H-induced defects in metals, the nature of the H-induced defects and the mechanism of their creation are still not completely understood. For these reasons the understanding of hydrogen interaction with defects is important for the development of new materials for hydrogen technologies.

Palladium (Pd) is widely used as a model system for investigations of hydrogen in metal lattice since Pd above the critical temperature of ~ 295 °C can absorb a relatively large amount of hydrogen ($x \sim 1$ H/Pd) and it can be easily charged with hydrogen [106, 107]. Moreover, Pd is used as gate electrodes of metal-oxide-semiconductor hydrogen sensors and hydrogen diffusion membranes [108–111].

Hydrogen absorbed in Pd forms an interstitial solid solution in the fcc Pd lattice, the so called α-phase, and causes a remarkable isotropic volume expansion [106]. It is known that hydrogen can be trapped at open volume defects like vacancies [101, 105], dislocations [109, 112] and grain boundaries [101, 113]. This can be explained by positive binding energy of hydrogen to defect, i.e. hydrogen attached to defect exhibits lower energy than hydrogen located at octahedral interstitial site [105]. The hydrogen solubility in the α-phase decreases at lower temperatures and the Pd–H system becomes a mechanical mixture of two phases in a certain range of hydrogen concentration: the α-phase with lower hydrogen content and the hydrogen-rich α'-phase [107]. Both the α-phase and α'-phase have the fcc structure and differ by hydrogen content only – by the average number of octahedral sites in the fcc Pd lattice occupied by hydrogen [105]. Since the absorbed hydrogen causes a considerable volume expansion the lattice parameter in the hydrogen-rich α'-phase is significantly higher than in the α-phase. In bulk Pd (α-phase), the maximum solubility of hydrogen at ~ 25 °C, expressed as the H/Pd ratio, is $c_H = 0.017$, while the α-phase and α'-phase co-exist up to ~ 0.58 H/Pd [105, 107].

Absorbed hydrogen is released from Pd if the sample is heated [114–116]. Differential scanning calorimetry (DSC) was employed by author of this work and co-authors (see Ref. [P17]) for the investigation of hydrogen desorption from Pd electrochemically charged with hydrogen. Hydrogen desorption from well annealed Pd polycrystals and plastically deformed Pd samples containing high density of dislocations was compared to elucidate the effect of dislocations on hydrogen desorption [P17]. The hydrogen desorption led to a pronounced endothermic peak in the DSC signal. The heat of hydrogen desorption was calculated as ~ 26 kJ/(mol H_2). If the environment of the measured sample contains oxygen, the endothermic desorption peak is followed by a strong exothermic peak caused by the heat released during fusion of desorbed hydrogen with oxygen and formation of water vapour. The comparison of

well annealed and plastically deformed Pd samples revealed that dislocations trap hydrogen atoms and suppress mobility of hydrogen atoms diffusing to the surface. As a consequence the hydrogen desorption peak was shifted to higher temperatures [P17].

Hydrogen-loaded films often behave very differently from the corresponding bulk materials [101]. It happens because of two main reasons: (i) contrary to free standing bulk samples which exhibit isotropic lattice expansion when loaded with hydrogen, thin films are clamped to a substrate. The clamping prevents the in-plane lattice expansion and causes appearance of large in-plane compressive stresses (in the GPa range) [117], which influence the behaviour of the loaded films. (ii) Films often exhibit a high density of lattice defects. This makes expansion of the film loaded with hydrogen strongly anisotropic: the in-plane expansion is suppressed, while the out-of-plane expansion is remarkably larger than in a free standing bulk metal.

Investigations of Pd films deposited on various substrates revealed that crystal structure of the substrate has relatively low impact on behaviour of the film loaded with hydrogen [118]. The dominating factor affecting the behaviour of hydrogen loaded film seems to be the strength of binding between the film and the substrate.

Different types of Pd films as a model system for investigation of structural changes caused by absorbed hydrogen were presented in this habilitation thesis. The Pd samples were usually step-by-step loaded with hydrogen by electrochemical charging in a galvanic cell filled with an electrolyte. The hydrogen concentration in the sample then can be calculated from the Faraday's Law. An inert protective atmosphere was used to prevent hydrogen loss by reaction with atmospheric oxygen.

I. Nanocrystalline Pd films

a. Pd films on sapphire substrate

Thin nanocrystalline Pd films (thickness about ~ 490 nm and ~ 1080 nm) were prepared in an UHV chamber (10^{-10} mbar) using cathode beam sputtering at room temperature on optically polished sapphire substrates – see Refs. [P18–P20].

TEM revealed the presence of ''column-like'' elongated grains with a lateral width around 50 nm in the virgin samples. Two kinds of columns were distinguished [P18, P19]: (i) "first generation columns" with average height of ~ 200 nm growing directly on the sapphire surface and (ii) "second generation columns" growing on the top of the first generation. The studies of microstructure revealed that formation of the α'-phase in the film started at $c_H \sim 0.03 – 0.10$ while the corresponding concentration for a bulk Pd single crystal is 0.017 only. The films exhibited higher hydrogen solubility in the α-phase – a high volume fraction of grain boundaries which contain open-volume defects can accumulate more hydrogen than a regular lattice.

Buckling of the film occurs at a certain critical concentration of absorbed hydrogen when the stored elastic strain energy overcomes the adhesion energy and hydrogen-induced stresses cause crack formation at the interface between the film and the substrate [111]. In the nanocrystalline Pd film the buckling started at $c_H > 0.05$ by the formation of straight buckles in the film and took place at the concentration range where the α- and α'-phase co-exist in the film. Formation of the α'-phase introduced new defects, but an increase of the defect density observed in the films is connected with the onset of buckling and most probably not with the

beginning of the α'-phase formation (see Refs. [P18–P20]). Since a straight buckle can release the in-plane stress in a one direction only [119] it is forced to expand also in the perpendicular direction and straight buckles become curved at later stages of buckling. A complicated pattern of many buckles of undulated shape was formed in the films loaded up to a hydrogen concentration $c_H > 0.3$.

It was also shown that the number of acoustic emission (AE) counts increases drastically, where the buckling process starts as the consequence of a collective movement of dislocations created during buckling of the film [P18, P19]. It was evident that parts of the film which were detached from the substrate become free and their in-plane expansion was not suppressed by the substrate anymore. Further hydrogen charging led to a complete detachment of the nanocrystalline film from the substrate [P18, P19].

b. Pd films on polystyrene and on silicon single crystal

Thin nanocrystalline Pd films (~ 500 nm) were prepared in a UHV chamber (10^{-10} mbar) using cathode beam sputtering at room temperature on polystyrene substrates and a silicon single crystal – see Ref. [P20].

The virgin Pd film on polystyrene substrate exhibited a higher out-of-plane lattice parameter than the lattice parameter of bulk Pd. This indicates that the film suffers from a bi-axial compressive in-plane stress imposed by the substrate. Hydrogen absorption firstly causes out-of-plane expansion. At higher hydrogen concentrations the lattice constant of the α-phase reaches plateau value and hydrogen rich α'-phase becomes detectable at $c_H \sim 0.23$. The lattice constant of the α-phase was observed significantly higher than the lattice constant for perfect bulk Pd crystal. And the out-of-plane lattice constant of the α'-phase during the phase transition was observed lower than the lattice constant of bulk α'-phase. The same results were obtained on the sapphire substrates (see above and/or Ref. [P19]). Two phase field ends at the concentration $c_H \sim 0.43$. Buckling of the film started at a hydrogen concentration $c_H \sim 0.09$ and, finally, the film was completely detached from the substrate at the end of the measurements. The observed increase of the solubility limit with respect to the bulk Pd is attributed to the nanocrystalline structure with a high volume fraction of grain boundaries which can absorb more hydrogen than the grain interiors.

The virgin Pd film on silicon single crystal also exhibited compressive in-plane stress as the film on polystyrene substrate. However, the peak-to-background ratio was observed clearly higher than for the film deposited on the polystyrene substrate (probably due to more developed texture). Buckling of the film was firstly observed at $c_H \sim 0.16$ but some portion of the film remains attached to the substrate up to the end of loading. The α-phase remained visible up to very high hydrogen concentrations – the apparent width of the two phase field was considerably higher in the Pd film deposited on Si substrate than in the Pd film on polystyrene substrate.

The conclusion of it is that the influence of polystyrene substrate on the stress state in Pd film is very low due to low Young's modulus of polystyrene and, more importantly, the low adhesion of the Pd film to the polystyrene than silicon (or sapphire) substrate.

This part of the presented work includes four original papers. See followed publications (Refs. [P17–P20]) at the end of the habilitation thesis (*Attached publications*):

[P17] Vlach M., Cizek J., Melikhova O., Kodetova V., Stulikova I.: *Hydrogen trapping at defects in Pd and thermally activated desorption*, DIFFUSION IN SOLIDS AND LIQUIDS X (eds.: Ochsner A., Murch G. E., Shokuhfar A., Delgado J. M. P. Q.), DEFECT AND DIFFUSION FORUM 365 (2015), p. 36.

[P18] Čížek J., Procházka I., Vlach M. et al.: *Hydrogen-induced buckling of Pd films studied by positron annihilation,* APPLIED SURFACE SCIENCE 255 (2008) 1, p. 241.

[P19] Cizek, J., Melikhova O., Vlcek M., Lukac F., Vlach M. et al.: *Hydrogen-induced microstructural changes of Pd films*, INTERNATIONAL JOURNAL OF HYDROGEN ENERGY 38 (2013) 27, p. 12115.

[P20] Vlcek M., Lukac F., Vlach M. et al.: *Influence of microstructure and mechanical stress on behaviour of hydrogen in 500 nm Pd films*, JOURNAL OF ALLOYS AND COMPOUNDS 645 (2015), p. S446.

II. Polycrystalline Pd films on sapphire substrate

Thin polycrystalline Pd films (thickness ~ 1040 nm) were prepared in a UHV chamber (10^{-10} mbar) using cathode beam sputtering at room temperature on optically polished sapphire substrate and then annealed in the UHV chamber at 800 °C/60 min – see Ref. [P19].

Microstructure observation showed that the high temperature annealing (800 °C/60 min) led to a polycrystalline structure with grain size around ~ 2.5 μm. Moreover the profile of the $(111)_{Pd}$ reflection measured by XRD for the polycrystalline films became symmetrical and can be well described by a single contribution (XRD studies were carried out by author of this work using synchrotron in HASYLAB, DESY, Germany at a beamline equipped with a four-axis Eulerian cradle). It testified that recrystallization took place in the whole film and wiped out differences between the first and the second generation crystallites (e.g. observed in the nanocrystalline films – see above). The out-of-plane lattice constant *a* was determined for the virgin polycrystalline film as ~ 3.870 Å. The value of it is smaller than the bulk Pd [109]. Hence, contrary to the nanocrystalline Pd film, the polycrystalline film exhibits tensile in-plane stress which is caused by lower thermal expansion of sapphire substrate compared to Pd. During annealing at elevated temperature when recrystallization takes place, Pd atoms are arranged into configuration with higher inter-atomic spacing corresponding to the elevated temperature. Since the thermal expansion of the sapphire substrate is lower than that of Pd, shrinkage of the Pd lattice during cooling of the film from elevated temperatures is hindered by the substrate leading finally to residual tensile stress in the film at room temperature [120, 121]. XRD measurements also showed a development of texture caused by the annealing at 800 °C/60 min. In a polycrystalline film most of the grains grew parallel with the substrate, but contrary to nanocrystalline films, the lateral orientation of grains is not random and one orientation in the plane of the substrate is preferred.

In-situ measurements during the hydrogen loading of the polycrystalline Pd film also showed that the hydrogen-induced out-of-plane expansion was occurred. This behaviour is comparable with bulk Pd, but polycrystalline film exhibits higher hydrogen solubility in the α-phase than bulk Pd. However, the in-plane tensile stress imposed by the substrate the out-of-plane lattice parameter of the film remained lower than the one for a bulk Pd crystal up to a

hydrogen concentration of $c_H \sim 0.14$. Subsequently phase transition from α-phase to α'-phase took place. The phase boundary between the phases was shifted to a hydrogen concentration significantly higher than in a bulk Pd crystal. This was also caused by tensile in-plane stress in the polycrystalline film which leads to the out-of-plane lattice parameter lower than in bulk Pd.

In the polycrystalline film, buckles were formed at $c_H > 0.4$. The lattice parameter a monotonically increased up to this concentration and approached the value for α-phase in bulk $Pd_{c_H=0.017}$. It can be clearly concluded that the annealing at 800 °C/60 min improved the bonding of the Pd film to the sapphire substrate.

This part of the presented work includes one original paper. See followed publication (Ref. [P19]) at the end of the habilitation thesis (*Attached publications*):
[P19] Cizek, J., Melikhova O., Vlcek M., Lukac F., Vlach M. et al.: *Hydrogen-induced microstructural changes of Pd films*, INTERNATIONAL JOURNAL OF HYDROGEN ENERGY 38 (2013) 27, p. 12115.

III. Epitaxial Pd films on sapphire substrate and on glimmer

Pd films with a thickness of ~ 490 nm were epitaxially deposited on a single crystal Al_2O_3 (sapphire) substrate. The deposition was performed in a UHV chamber by cathode beam sputtering at substrate temperature of 800 °C – see Refs. [P19, P21].

In the virgin film, the profile of the $(111)_{Pd}$ reflection measured by XRD for the epitaxial films was observed clearly significantly narrower compared to the nanocrystalline films (XRD studies were carried out by author of this work using synchrotron in HASYLAB, DESY, Germany at a beamline equipped with a four-axis Eulerian cradle). The epitaxial films also exhibited a single orientation with respect to the substrate and an out-of-plane lattice parameter lower than in bulk Pd. It is known that epitaxial films contain an array of misfit dislocations, which accommodate the lattice mismatch between the film and the substrate [122]. In epitaxial Pd films it was observed that the density of misfit dislocations increases from the surface towards the film-substrate interface due to an increasing distortion of the film lattice and virgin Pd films contain besides misfit dislocations also larger vacancy clusters and/or voids [P19, P21].

New defects due to the hydrogen-induced volume expansion were introduced in the epitaxial Pd films by hydrogen loading and were formed already at low hydrogen concentrations ($c_H \sim 0.04$). The α-phase lattice parameter for the hydrogen loaded film increases and reaches the value for bulk Pd at $c_H \sim 0.06$, and then remains virtually constant during further loading. The α'-phase exhibited a lattice constant lower than the bulk value when it initially appeared. The dislocations were created by hydrogen loading either due to plastic deformation initiated by hydrogen-induced stresses and/or by precipitation of hydride particles. During further hydrogen loading the α'-phase lattice parameter firstly increases and stays constant with the value lower than the bulk value.

The high bonding strength of the epitaxial film deposited on sapphire substrate prevents buckling and inhibits the complete transformation of the film to the α'-phase. Since no buckling of the films was observed in the whole range of hydrogen concentrations examined in our works, e.g. [P19, P21], one can conclude that the best bonding of the Pd layer to the sapphire substrate was achieved in the epitaxial Pd film deposited at elevated temperature. This verifies a strong adhesion to the substrate for this type of films.

We also studied the epitaxial Pd films deposited on a glimmer substrate (see Ref. [123]) where the α'-phase grew in layers starting from the film surface and gradually extending deeper into the film. The epitaxial film deposited on the glimmer substrate exhibited a lower bonding strength and detached from the substrate during hydrogen loading. The buckling was also observed. More relevant information can be found in Ref. [123].

This part of the presented work includes two original papers. See followed publications (Refs. [P19, P21]) at the end of the habilitation thesis (*Attached publications*):
[P19] Cizek J., Melikhova O., Vlcek M., Lukac F., Vlach M. et al.: *Hydrogen-induced microstructural changes of Pd films*, INTERNATIONAL JOURNAL OF HYDROGEN ENERGY 38 (2013) 27, p. 12115.
[P21] Čížek J., Procházka I., Melikhova O., Vlach M. et al.: *Hydrogen-induced defects in Pd films*, PHYSICA STATUS SOLIDI C – SOLID STATE PHYSICS 6 (2009) 11, p. 2364.

IV. Very thin Pd films

It has been reported that in very thin films (~ the tens of nm thick films) the relaxation mechanisms are energetically unfavourable and hydride precipitates stay coherent with the α'-phase matrix [124, 125].

To investigate the critical thickness of the Pd films we studied selected very thin polycrystalline, nanocrystalline and epitaxial Pd films (~ 25 nm of the thickness) deposited on sapphire (see Refs. [P22, P23]). Hydrogen loading was performed at room temperature from the hydrogen gas using the pressure range from 10^{-2} to 900 mbar. Changes of the lattice parameter and of the interface roughness of the hydrogen loaded films were measured in situ with X-ray diffraction (XRD) at synchrotron radiation facilities at Grenoble (ESRF, Beamline BM 20 operated by the HZDR, Germany) and/or Hamburg (HASYLAB, DESY, Beamline B2).

Our published study (Ref. [P22]) on very thin polycrystalline Pd films showed the existence of a critical thickness, where the α'-phase precipitates stayed coherent with the α-matrix throughout complete phase transition in Pd thin films on sapphire. We also found that the critical film thickness for coherent phase transition is below ~ 34 nm, but above ~ 22 nm Pd film thicknesses – the larger overall out-of-plane expansion of the 22.5 nm Pd film compared to the 34 nm film revealed different magnitudes of in-plane stress relaxation. Consequently, for the thicker films the thickness fringes did not reappear during unloading as more material had been transported to the film surface. At film thicknesses above ~ 22 nm, misfit dislocation loop formation around α'-phase precipitates became possible. Above this thickness, the hydride phase relaxes towards the substrate and towards the α-phase. Above ~ 100 nm thickness, films can also detach from the substrate [P22].

Recently we also verified the coherent state in very thin epitaxial and nanocrystalline Pd films with thickness below the critical value (~ 20 nm) – see Ref. [P23]. The nanocrystalline films suffered from in-plane compressive stress imposed by atomic preening processes. The epitaxial films exhibited tensile stress caused by the different thermal expansion coefficients of Pd and sapphire substrate. For both films, the lattice parameters continuously increased during the phase transition to the α'-phase. Both films exhibited enhanced hydride formation pressure compared to bulk Pd. Misfit dislocations were formed at interface between Pd films and

substrate during hydrogenation. This led to irreversible change of stress state of the films subjected to sorption and desorption cycle with hydrogen.

This part of the presented work includes two original papers. See followed publications (Refs. [P22, P23]) at the end of the habilitation thesis (*Attached publications*):

[P22] Wagner S., Uchida H., Burlaka V., Vlach M. et al.: *Achieving coherent phase transition in palladium-hydrogen thin films*, SCRIPTA MATERIALIA 64 (2011) 10, p. 978.

[P23] Lukac F., Vlcek M., Vlach M. et al.: *Stress release during cyclic loading of 20 nm palladium films*, JOURNAL OF ALLOYS AND COMPOUNDS 645 (2015), p. S450.

Summary

The detailed investigation of precipitation processes in: a) the as-cast and differently deformed Al–Mn, Al–Sc–Zr and Al–Mn–Sc–Zr alloys and alloys with substantial grain refinement (prepared by powder metallurgy) alloyed with various combinations of Mn, Sc and Zr; b) the squeeze-cast, solution-treated, and severe plastic deformed Mg–Tb and Mg–Tb–Nd alloys, and Mg–Tb–Nd alloy with substantial grain refinement (prepared by powder metallurgy); and c) the thin Pd films during hydrogen loading were carried out.

The habilitation thesis was based on a compilation of 23 peer-reviewed articles published in international journals. The results were presented at international conferences and scientific seminars of the Charles University Research Centre (UNCE). In order to obtain complex information about the materials studied and to simplify the interpretation of obtained results, the electrical resistivity measurements with Vickers microhardness measurements and differential scanning calorimetry were often combined. In addition, the positron annihilation spectroscopy, structure and microstructure analysis by transmission electron microscopy, electron diffraction, X-ray microanalysis, electron back-scattered diffraction, scanning electron microscopy and small angle X-ray scattering were used. Last but not least the work deepens an international co-operation.

From the presented results it can be concluded:

- Peak hardening in the Al–Sc–Zr alloy and Al–Mn–Sc–Zr alloys is caused by precipitation of the Al_3Sc and/or $Al_3(Sc,Zr)$ particles. The development of the particles is slightly facilitated by the previous type of deformation.
- The precipitation of the Mn-containing particles in the Al-based alloys depends on the deformation degree in the studied alloys – the higher deformation the more intensive precipitation of the $Al_6(Mn,Fe)$ particles. Unlike precipitation of the Sc-containing particles the Al_6Mn precipitation is highly enhanced by a deformation. Nevertheless, the precipitation of these particles has an insignificant effect on hardness in all the studied alloys.
- The deformation of the Al(–Mn)–Sc–Zr alloys has no effect on the apparent activation energy values. However, the deformation affects the temperature range of the phase transformations.
- The Mn-addition does not influence the decomposition of the Al–Sc–Zr system. However, the texture development of the Al–Sc–Zr-based alloys during preparation seems to be affected by high solid solution strengthening by Mn.
- To the author's knowledge the positron annihilation spectroscopy was in the Al–Sc- and/or Al–Zr-based alloys used for the first time. Clustering of Sc solute occurs at temperatures above ~ 150 °C. Sc-rich regions are associated with vacancies particularly in the early stages of their formation. Zr solutes migration starts above ~ 240 °C contributing to the development of the Sc,Zr-containing particles.
- Two precipitation stages of the Mn-containing particles during isochronal annealing were observed in the deformed Al–Mn–Sc–Zr alloys: i) the Al_6Mn particles at (sub)grain boundaries at ~ 320 °C, ii) the Mn-rich particles inside (sub)grain interior after annealing up to 400 °C.

- The presence of the $Al_3(Sc,Zr)$ particles has a significant antirecrystallization effect and prevents recrystallization minimally up to 420 °C in the Al-based alloys.
- The suitable mix of nano-sized Sc,Zr-containing dispersoids and coarse Mn-containing particles totally suppresses recrystallization at 550 °C in the Al-based alloys with substantial grain refinement.

- Isothermal resistivity annealing curve at 530 °C for the binary Mg–Tb alloy approaches the saturated resistivity values for reasonable times (~ 4 hours) showing the possibility to quench in the supersaturated solid solutions. During solution treatment some thermal vacancies form pairs with solute atoms in the Mg–Tb alloy.
- The hardness of the solution-treated Mg–Tb alloy aged at room temperature rises due to formation of small clusters of Tb atoms. Quenched-in vacancies facilitate clustering of Tb solutes and disappear from the samples when the clusters are fully developed. It was found that natural aging of Mg–Tb alloy has beneficial effect on hardening by β'' phase particles formed during subsequent annealing.
- Comparison of precipitation processes in the Mg–Tb alloy in solution-treated state and HPT-deformed sample revealed that precipitation is enhanced in the HPT-deformed alloy due to the higher diffusivity of Mg and Tb atoms and due to the high density of nucleation centres for the second phase particles. As a consequence, precipitation of metastable phases occurs at lower temperatures in HPT-deformed samples than in common coarse-grained (solution-treated) alloys.
- Isothermal resistivity annealing curve at 500 °C for the ternary Mg–Tb–Nd alloy approaches the saturated resistivity values for reasonable times (~ 4 hours) showing the possibility to quench in the supersaturated solid solutions.
- Three transient and two stable phases precipitate sequentially during the isochronal annealing in the studied Mg–Tb–Nd alloys. The precipitation sequence includes successively ($D0_{19}$ clusters,) $D0_{19}$ particles, extremely small particles of the β' phase, β_1 phase with fcc structure, β phase of $Mg_5(Tb,Nd)$ type and β_e phase of $Mg_{41}(Tb,Nd)_5$ type.
- The precipitation of the β_1 phase starts at remarkably lower temperatures on the precipitation sequence in the Mg–Tb–Nd alloy with UFG structure (compared to the coarse-grained/solution-treated alloy).
- The initial structure of the Mg–Tb–Nd alloy prepared by powder metallurgy (PM) is partly recrystallized with (sub)grains size not exceeding ~ 5 μm. Hardening due to isochronal annealing is negligible in the PM alloy contrary to the solution-treated alloy, as contributions of structure and precipitation effects to hardness do not add linearly and volume fraction of precipitated phases is not the same in these materials due to a different supersaturation.
- Powder metallurgy way of alloy preparation changes neither the precipitation sequence in the Mg–Tb–Nd alloy nor activation energy values of the particular precipitation processes but shifts temperature ranges of these processes.

- Hydrogen-induced plastic deformation took place in Pd films studied; it introduced new defects into the Pd films.
- The critical thickness value in thin Pd films was observed. At film thicknesses above about 22 nm, misfit dislocation loop formation around hydride precipitates becomes

possible. Above this thickness, the hydride phase relaxes towards the substrate and towards the α-phase. Above 100 nm thickness, films can also detach from the substrate (so called "buckling").

- In the nanocrystalline film, buckling occurs at hydrogen concentrations $c_H > 0.05$, while in the polycrystalline films annealed at 800 °C the binding of Pd atoms with the sapphire substrate was improved and the start of buckling was shifted to higher hydrogen concentrations $c_H > 0.4$.
- Adhesion of nanocrystalline Pd films to the silicon substrate is higher than for the film deposited on the polystyrene substrate which buckles very easily. The deviations from the behaviour of bulk Pd in the film deposited on polystyrene substrate are mainly attributed to its nanocrystalline structure, while in the film deposited on silicon substrate, both nanocrystalline grain size and stresses induced by silicon substrate play an important role.
- The epitaxial films deposited at elevated temperature exhibits the best binding to the sapphire substrate. No buckling of this film has been observed.

References

[1] http://www.roskill.com/reports/aluminium (position as per March 2nd, 2016).
[2] http://www.zelenykruh.cz/dokumenty/ceska-stopa.pdf (position as per March 2nd, 2016).
[3] Schuman S., Friedrich F.: The use of magnesium in cars – today and in future, in: MAGNESIUM ALLOYS AND THEIR APPLICATIONS (eds.: Mordike B. L., Kainer K. U.), Werkstoff-Informationsgesselschaft, Frankfurt, 1998.
[4] Jones M. J., Humphreys F. J.: ACTA MATERIALIA 51 (2003), p. 2149.
[5] Davydov V. G., Rostova T. D., Zakharov V. V., Filatov Y. A., Yelagin V. I.: MATERIALS SCIENCE AND ENGINEERING A-STRUCTURAL MATERIALS PROPERTIES MICROSTRUCTURE AND PROCESSING 280 (2000), p. 30.
[6] Toropova L. S., Eskin D. G., Kharakterova M. L., Dobatkina T. V.: Advanced Aluminium Alloys Containing Scandium – Structure and Properties, Gordon and Breach Science Publisher, The Netherlands, 1998.
[7] Liu J., Yao P., Zhao N et al.: JOURNAL OF ALLOYS AND COMPOUNDS 657 (2016), p. 717.
[8] Baba Y., Takashima A.: MATERIALS TRANSACTIONS (JIM) 10 (1969), p. 196.
[9] Røyset J., Stene T., Saeter J. A., Reiso O: MATERIALS SCIENCE FORUM 519 (2006), p. 239.
[10] Røyset J., Ryum R.: INTERNATIONAL MATERIALS REVIEW 50 (2005), p. 19.
[11] Booth-Morrison C., Dunand D. C., Seidman D. N.: ACTA MATERIALIA 59 (2011), p. 7029.
[12] Clouet E., Barbu A.: ACTA MATERIALIA 55 (2007), p. 391.
[13] Lefebvre W., Danoix F., Hallem H., Forbord B., Bostel A., Marthinsen K.: JOURNAL OF ALLOYS AND COMPOUNDS 470 (2009), p. 107.
[14] Neubert V., Smola B., Stulikova I., Bakkar A., Reuter J.: MATERIALS SCIENCE AND ENGINEERING A-STRUCTURAL MATERIALS PROPERTIES MICROSTRUCTURE AND PROCESSING 464 (2007), p. 358.
[15] Marquis E. A., Seidman D. N.: ACTA MATERIALIA 49 (2001), p. 1909.
[16] Norman A. F., Prangnell P. B., McEwen R. S.: ACTA MATERIALIA 46 (1998), p. 5715.
[17] Seidman D. N., Marquis E. A., Dunand D. C.: ACTA MATERIALIA 50 (2002), p. 4021.
[18] Zhou W. W., Cai B., Li W. J., Liu Z. X., Yang S.: MATERIALS SCIENCE AND ENGINEERING A-STRUCTURAL MATERIALS PROPERTIES MICROSTRUCTURE AND PROCESSING 552 (2012), p. 353.
[19] Belov N. A., Alabin A. N., Matveeva I. A.: JOURNAL OF ALLOYS AND COMPOUNDS 583 (2014), p. 206.
[20] Forbord B., Lefebvre W., Danoix F., Hallem H., Marthinsen K.: SCRIPTA MATERIALIA 51 (2004), p. 333.
[21] De Luca A., Dunand D. C., Seidman D. N.: ACTA MATERIALIA 119 (2016), p. 35.
[22] Rossiter P. L.: The Electrical Resistivity of Metals and Alloys, Cambridge University Press, United Kingdom, 1987.
[23] Doyama M., Koehler J. S.: PHYSICAL REVIEW 134 (1964), no. A522.
[24] Carling K. M., Wahnstrom G., Mattsson T. R., Sandberg N., Grimvall G.: PHYSICAL REVIEW B 67 (2003), no. 054101.
[25] Dalen v. M. E., Seidman D. N., Dunand D. C.: ACTA MATERIALIA 56 (2008), p. 4369.
[26] Knipling K. E., Dunand D. C., Seidman D. N.: ACTA MATERIALIA 56 (2008), p. 1182.
[27] Knipling K. E., Dunand D. C., Seidman D. N.: INTERNATIONAL JOURNAL OF MATERIALS RESEARCH 97 (2006), p. 246.
[28] Lodgaard L., Ryum N.: MATERIALS SCIENCE AND ENGINEERING A-STRUCTURAL MATERIALS PROPERTIES MICROSTRUCTURE AND PROCESSING 283 (2000), p. 144.
[29] Jia Z., Røyset J., Solberg J. K., Liu Q.: TRANSACTIONS OF NONFERROUS METALS SOCIETY OF CHINA 22 (2012), p. 1866.
[30] Jaradeh M. M. R., Carlberg T.: JOURNAL OF MATERIALS SCIENCE & TECHNOLOGY 27 (2011), p. 615.
[31] Zhou Z., Wu B., Dou S. et al.: METALLURGICAL AND MATERIALS TRANSACTIONS A-PHYSICAL METALLURGY AND MATERIALS 45A (2014), p. 1720.

[32] Forbord B., Auran L., Lefebvre W., Hallem H., Marthinsen K.: MATERIALS SCIENCE AND ENGINEERING A-STRUCTURAL MATERIALS PROPERTIES MICROSTRUCTURE AND PROCESSING 424 (2006), p. 174.
[33] Riddle Y. W., Hallem H., Ryum R.: MATERIALS SCIENCE FORUM 396–402 (2002), p. 563.
[34] Karlík M., Slámová M., Mánik T.: KOVOVE MATERIALY-METALLIC MATERIALS 47 (2009), p. 139.
[35] Raghavan V.: JOURNAL OF PHASE EQUILIBRIA AND DIFFUSION 30 (2009), p. 191.
[36] Jo H., Fujikawa S. I.: MATERIALS SCIENCE AND ENGINEERING A-STRUCTURAL MATERIALS PROPERTIES MICROSTRUCTURE AND PROCESSING 171 (1993), p. 151.
[37] Fan K., Liu F., Zhang K., Yang G. C., Zhou Y. H.: JOURNAL OF CRYSTAL GROWTH 311 (2009), p. 4660.
[38] Xia X.: SCRIPTA METALLURGICA 28 (1993), p. 1213.
[39] Birol Y: SCRIPTA MATERIALIA. 60 (2009), p. 5.
[40] Du Y., Wang J., Zhao J. et al.: INTERNATIONAL JOURNAL OF MATERIALS RESEARCH 98 (2007), p. 855.
[41] Cieslar M., Slámová M., Uhlíř J., Coupeau C., Bonneville J.: KOVOVE MATERIALY-METALLIC MATERIALS 45 (2007), p. 91.
[42] Forbord B., Hallem H., Røyset J., Marthinsen K.: MATERIALS SCIENCE AND ENGINEERING A-STRUCTURAL MATERIALS PROPERTIES MICROSTRUCTURE AND PROCESSING 475 (2008), p. 241
[43] Knipling K. E., Karnesky R. A., Lee C. P., Dunand D. C., Seidman D. N.: ACTA MATERIALIA 58 (2010), p. 5184.
[44] Nes E.: ACTA METALLURGICA 24 (1976), p. 391.
[45] Nes E., Ryum N., Hunderi O.: ACTA METALLURGICA 33 (1985), p. 11.
[46] Roumina R., Sinclair C. W.: ACTA MATERIALIA 58 (2010), p. 111.
[47] Nes E.: ACTA METALLURGICA 43 (1995), p. 2189.
[48] Karnowsky M. M., Moss M., Stein C.: SCRIPTA METALLURGICA 8 (1974), p. 513.
[49] Luiggi N. J.: METALLURGICAL AND MATERIALS TRANSACTIONS B-PROCESS METALLURGY AND MATERIALS PROCESSING SCIENCE 28 (1997), p. 149.
[50] Kendig K. L., Miracle D. B.: ACTA MATERIALIA 50 (2002), p. 4165.
[51] Fuji H., Sugamata M., Kaneko J., Kubota M.: MATERIALS SCIENCE FORUM 396–402 (2002), p. 245.
[52] Smola B., Stulíková I., Očenášek V., Pelcová J., Neubert V.: MATERIALS SCIENCE AND ENGINEERING A-STRUCTURAL MATERIALS PROPERTIES MICROSTRUCTURE AND PROCESSING 462 (2007), p. 370.
[53] Kolář M., Očenášek V., Uhlíř J. et al.: MATERIALS SCIENCE FORUM 567–568 (2008), p. 357.
[54] Vlach M., Stulíková I., Smola B. et al.: ACTA PHYSICA POLONICA A 122 (2012), p. 439.
[55] Karlik M., Manik T., Slamova M., Lauschmann H.: ACTA PHYSICA POLONICA A 122 (2012), p. 469.
[56] Vo N. Q., Dunand D. C., Seidman D. N.: ACTA MATERIALIA 63 (2014), p. 73.
[57] Vlach, M., Stulikova, I., Smola, B. et al.: DEFECT AND DIFFUSION FORUM 334–335 (2013), p. 161.
[58] Mordike B. L., Ebert T.: MATERIALS SCIENCE AND ENGINEERING A-STRUCTURAL MATERIALS PROPERTIES MICROSTRUCTURE AND PROCESSING 302 (2001), p. 37.
[59] Smola B., Stulíková I.: JOURNAL OF ALLOYS AND COMPOUNDS 381 (2004), p. L1.
[60] Roklin L. L.: Magnesium Alloys Containing Rare Earth Metals, Taylor & Francis, London, 2003.
[61] Polmear I. J.: Light Alloys (3rd ed.), Edward Arnold, London, 1995.
[62] Lorimer G. W.: Proc. London Conf. Magnesium Technology (ed.: Baker H.), Inst. Of Metals, London, 1986, p. 47.
[63] Vostry P., Stulikova I., Smola B., Cieslar M., Mordike B. L.: ZEITSCHRIFT FUR METALLKUNDE 79 (1988), p. 340.

[64] Smola B., Stulíková I., Buch v. F., Mordike B. L.: MATERIALS SCIENCE AND ENGINEERING A-STRUCTURAL MATERIALS PROPERTIES MICROSTRUCTURE AND PROCESSING 324 (2002), p. 113.
[65] Mordike B. L., Stulíková I., Smola B.: METALLURGICAL AND MATERIALS TRANSACTIONS A-PHYSICAL METALLURGY AND MATERIALS 36A (2005), p. 1729.
[66] Staiger M. P., Pietak A. M., Huadmai J., Dias G.: BIOMATERIALS 27 (2006), p. 1728.
[67] Witte F., Kaese V., Haferkamp H. et al.: BIOMATERIALS 26 (2005), p. 3557.
[68] Hänzi A. C., Gunde P., Schinhammer M., Uggowitzer P. J.: ACTA BIOMATERIALIA 5 (2009), p. 162.
[69] Witte F., Hort N., Vogt C. et al.: CURRENT OPINION IN SOLID STATE & MATERIALS SCIENCE 12 (2008), p. 63.
[70] Yun Y. H., Dong Z., Yang D.: MATERIALS SCIENCE AND ENGINEERING C: MATERIALS FOR BIOLOGICAL APPLICATIONS 29 (2009), p. 1814.
[71] Nie J. F.: METALLURGICAL AND MATERIALS TRANSACTIONS A-PHYSICAL METALLURGY AND MATERIALS 43A (2012), p. 3891.
[72] Nie J. F., Muddle B. C.: ACTA MATERIALIA 48 (2000), p. 1691.
[73] Antion C., Donnadieu P., Perrard F. et al: ACTA MATERIALIA 51 (2003), p. 5335.
[74] Xu Z., Weyland M., Nie J. F.: ACTA MATERIALIA 81 (2014), p. 58.
[75] Li D., Dong J., Zeng X., Lu C.: MATERIALS CHARACTERIZATION 61 (2010), p. 818.
[76] Riontino G., Lussana D., Massazza M.: JOURNAL OF THERMAL ANALYSIS AND CALORIMETRY 83 (2006), p. 643.
[77] Riontino G., Lussana D., Massazza M., Barucca G., Mengucci P., Ferragut R.: JOURNAL OF ALLOYS AND COMPOUNDS 463 (2008), p. 200.
[78] Nie J. F.: SCRIPTA MATERIALIA 48 (2003), p. 1009.
[79] Pike T. J., Noble B.: JOURNAL OF THE LESS COMMON METALS 30 (1973), p. 63.
[80] Ferragut R., Moia F., Fiori F., Lussana D., Riontino G.: JOURNAL OF ALLOYS AND COMPOUNDS 495 (2010), p. 408.
[81] Cabeza S., Garces G., Perez P., Adeva P.: THE JOURNAL OF THE MECHANICAL BEHAVIOR OF BIOMEDICAL MATERIALS 46 (2015), p. 115.
[82] Zhang H. J., Zhang D. J., Ma C. H., Guo S. F.: MATERIALS LETTERS 92 (2013), p. 45.
[83] Valiev R. Z., Islamgaliev R. K., Alexandrov I. V.: PROGRESS IN MATERIALS SCIENCE 45 (2000), p. 103.
[84] Zhilyaev A. P., Langdon T. G.: PROGRESS IN MATERIALS SCIENCE 53 (2008), p. 893.
[85] Čížek J., Procházka I., Smola B. et al.: MATERIALS SCIENCE FORUM 633–634 (2010), p. 353.
[86] Čížek J., Procházka I., Smola B. et al.: PHYSICA STATUS SOLIDI A-APPLICATIONS AND MATERIALS SCIENCE 203 (2006), p. 466.
[87] Esmaeili S., Lloyd D. J., Poole W. J.: ACTA MATERIALIA 51 (2003), p. 3467.
[88] Ohkubo H., Shimomura Y., Mukouda I., Sugio K., Kiritani M.: MATERIALS SCIENCE AND ENGINEERING A-STRUCTURAL MATERIALS PROPERTIES MICROSTRUCTURE AND PROCESSING 350 (2003), p. 30.
[89] Riedl A., Schwellinger P., Bichsel H.: ALUMINIUM 53 (1977), p. 595.
[90] Chang C. S. T., Wieler I., Wanderka N., Banhart J.: ULTRAMICROSCOPY 109 (2009), p. 585.
[91] Marceau R. K. W., de Vaucorbeil A., Sha G., Ringem S. P., Poole W. J.: ACTA MATERIALIA 61 (2013), p. 7285.
[92] Marceau R. K. W., Stephenson L. T., Hutchinson C. R., Ringer S. P.: ULTRAMICROSCOPY 111 (2011), p. 738.
[93] Pogatscher S., Antrekowitsch H., Leitner H., Ebner T., Uggowitzer P. J.: ACTA MATERIALIA 59 (2011), p. 3352.
[94] Pashley D. W., Rhodes J. W., Sendorek A.: JOURNAL OF THE INSTITUTE OF METALS (JIMEA) 94 (1966), p. 41.
[95] Buha J.: JOURNAL OF MATERIALS SCIENCE 43 (2008), p. 1120.
[96] Buha J.: ACTA MATERIALIA 56 (2008), p. 3533.
[97] Melikhova O., Cizek J., Hruska P. et al.: DEFECT AND DIFFUSION FORUM 333 (2013), p. 51.

[98] Tzanetakis P., Hillairet J., Revel G.: PHYSICA STATUS SOLIDI (B) - BASIC SOLID STATE PHYSICS 75 (1976), p. 433.
[99] Gemma R: unpublished results.
[100] Kumar P., Malhotra L.: MATERIALS CHEMISTRY AND PHYSICS 88 (2004), p. 106.
[101] Pundt A., Kirchheim: ANNUAL REVIEW OF MATERIALS RESEARCH 36 (2006), p. 555.
[102] Fukai Y., Ōkuma N.: JAPANESE JOURNAL OF APPLIED PHYSICS (JJAP) 32 (1993), p. L1256.
[103] Field R. D., Thoma D. J.: SRIPTA MATERIALIA 37 (1997), p. 347.
[104] Huiberts J. N., Griessen R., Rector J. H. et al.: NATURE 380 (1996), p. 231.
[105] Flanagan T. B., Oates W. A.: ANNUAL REVIEW OF MATERIALS RESEARCH 21 (1991), p. 269.
[106] Lewis F. A.: The Palladium Hydrogen System, Academic Press, London, 1967.
[107] Massalski T. B. (ed.): Binary Alloy Phase Diagrams, ASM, Metals Park, OH, 1993.
[108] Pick M., Davenport J. W., Strongin M., Dodnes G. J.: PHYSICAL REVIEW LETTERS 43 (1979), p. 286.
[109] Kircheim R.: PROGRESS IN MATERIALS SCIENCE 32 (1988), p. 261.
[110] Cizek J., Zaludova N., Vlach M. et al.: JOURNAL OF APPLIED PHYSICS 103 (2008), no. 053508.
[111] Lundström I., Shivaraman S., Svensson C.: APPLIED PHYSICS LETTERS 26 (1975), p. 55.
[112] Kirchheim R.: ACTA METALLURGICA 29 (1981), p. 835.
[113] Mütschele T., Kirchheim R.: SCRIPTA METALLURGICA 21 (1987), p. 135.
[114] Artman D., Flanagan T. B.: CANADIAN JOURNAL OF CHEMISTRY 50 (1972), p. 1321.
[115] Berlouis L. E. A., Hall P. J., MacKinnon A. J. et al.: JOURNAL OF ALLOYS AND COMPOUNDS 253-254 (1997), p. 207.
[116] Hirai N., Takashima M., Tahala T., Hara S.: SCIENCE AND TECHNOLOGY OF ADVANCED MATERIALS 5 (2004), p. 181.
[117] Laudahn U., Pundt A., Bicker M. et al.: JOURNAL OF ALLOYS AND COMPOUNDS 293–295 (1999), p. 490.
[118] Pundt A., Getzlaff M., Bode M. et al.: PHYSICAL REVIEW B 61 (2000), no. 9964.
[119] Yu Y., Kim C., Sanday S. C.: THIN SOLID FILMS 196 (1991), p. 229.
[120] Elomari S., Boukhili R., Lloyd D. J.: ACTA MATERIALIA 44 (1996), p. 1873.
[121] Waterhouse N., Yates B.: CRYOGENICS 8 (1968), p. 267.
[122] Wildes A. R., Mayer J., Theis-Bröhl K.: THIN SOLID FILMS 401 (2001), p. 7.
[123] Vlček M., Lukáč F., Vlach M. et al.: DEFECT AND DIFFUSION FORUM 365 (2015), p. 55.
[124] Pundt A.: ADVANCED ENGINEERING MATERIALS 6 (2004), p. 11.
[125] Nörthemann K., Pundt A.: PHYSICAL REVIEW B 78 (2008), no. 014105.

Slovo autora/Author's note

V tématice habilitačního spisu z pochopitelných důvodů nemohu zohlednit vlastní pedagogicko-popularizační činnost, která se mi však během odborné asistentury stala velkou vášní. Byl jsem například řešitelem projektu *Elektronický katalog fyzikálních demonstračních experimentů z mechaniky* v rámci FRVŠ (2012), spoluautorem scénáře vzdělávacího televizního seriálu *Rande s Fyzikou* (2011 – 2015) na ČT1, několika dílů pořadu pro děti *Zprávičky/Víte proč* (2014) na dětském kanále ČT:D či vedoucím projektu na *Záchranu rotundy sv. Václava na Malostranském náměstí v Praze* (2014 – 2016). Čas jsem věnoval i psaní učebnic a popularizačních knih, které se staly komerčně úspěšnými tituly (*Začínáme s LabVIEW*, *Rande s Fyzikou*, *Cesty nesmrtelných*).

Původně jsem chtěl psát habilitační spis v českém jazyce. Motivoval mě k tomu právě hluboký zájem o mapování života významných českých matematiků, fyziků a astronomů, kteří stáli u zrodu českého matematického a fyzikálního názvosloví, česky psaných gymnaziálních učebnic, českých školských reforem a české fyziky v jejím celku. Dalším důvodem je mé působení v Kabinetu výuky obecné fyziky MFF UK, díky kterému jsem začal věnovat pozornost také historickým souvislostem exaktní vědy. Přiznávám, že mimořádné a nelehké osudy českých fyziků ve mně vyvolávají pocit vlastenectví a sounáležitosti s těmi, kdo zasvětili mnohdy celý život boji za tak dobré podmínky pro českou akademickou fyziku, jaké máme nyní. Habilitační spis je však nakonec psán v jazyce současného vědeckého světa – v angličtině. K tomuto kroku jsem přistoupil ze zcela pragmatických důvodů. Dnes se česká fyzika bez publikování ve světovém jazyce prostě neobejde. Přesto mi dovolte alespoň na těchto místech vzdát hold těm „mnoha (často již) zapomenutým velikánům, na jejichž ramenech nyní stojíme". Tolik několik slov z pocitů autora v průběhu psaní práce.

For reasons that are obvious, the text of this habilitation thesis cannot include the results of my educational and popular-scientific activities, which have nevertheless become a great passion during my post-doc fellowship years. For instance, I was a solver in a HEDF/FRVŠ project "*Elektronický katalog fyzikálních demonstračních experimentů z mechaniky/Electronic Catalogue of Physical Demonstrational Experiments in Mechanics*" in 2012. I also co-authored several scripts of an educational Czech television (Channel 1) programme *Rande s Fyzikou* (2011 – 2015) and several episodes of a children's programme *Zprávičky/Víte proč* (2014) broadcast on the children's channel of the Czech Television ČT:D. I have been the head manager of the *Preservation Project of St. Wenceslas Rotunda at the Lesser Square Town in Prague* (2014 – 2016). I have also written several textbooks and popular science books that have become commercially successful (in Czech: *Začínáme s LabVIEW*, *Rande s Fyzikou*, *Cesty nesmrtelných*).

My initial idea was to write the habilitation thesis in the Czech language. It was largely conditioned by my leisure time activities that mapped the lives of the many Czech mathematicians, physicists and astronomers who witnessed the birth of the Czech mathematical and physical terminology, Czech physics or mathematics as a discipline, first Czech-language secondary school textbooks, and many other Czech educational reforms. Another reason for writing my thesis in Czech was my work at the Laboratory of the General Physics Education (Faculty of Mathematics and Physics, Charles University), thanks to which I came across the idea of mapping history. I must admit that initially it was perhaps the feeling of patriotism and the sense of solidarity with those who had to fight for the good conditions that the Czech academic physics was eventually able to create and maintain. Having read my habilitation thesis you will see that it was written in the language of contemporary scientific world – in English. Ultimately, I have chosen this approach for entirely pragmatic reasons: in today's world, Czech physics simply cannot do without publications in a universal language. Nevertheless, I would still like to take the present opportunity to pay homage to "the many (now often forgotten) giants on whose shoulders we are now standing". So much briefly for the author's thoughts in the course of the completing this work.

Attached publications

23 scientific peer-reviewed publications are attached. I am a corresponding author/first author on 10 of them. The selection is based on my research focus on the three different angles: a) precipitation process in Al-based alloys with the content of Sc and Zr; b) precipitation process in Mg-based alloys with rare earths addition; and c) the influence of hydrogen absorption on phase transformation in Pd films.

[P1] Vlach M., Stulíková I., Smola B., Žaludová N., Černá J.: *Phase transformations in isochronally annealed mould-cast and cold-rolled Al-Sc-Zr-based alloy*, JOURNAL OF ALLOYS AND COMPOUNDS 492 (2010) 1–2, p. 143. DOI: 10.1016/j.jallcom.2009.11.126.

[P2] Vlach M., Cizek J., Melikhova O. et al.: *Early Stages of Precipitation Process in Al-(Mn-)Sc-Zr Alloy Characterized by Positron Annihilation*, METALLURGICAL AND MATERIALS TRANSACTIONS A-PHYSICAL METALLURGY AND MATERIALS 46A (2015) 4, p. 1556. DOI: 10.1007/s11661-015-2767-x.

[P3] Vlach M., Stulikova I., Smola B. et al.: *Phase Transformations and Recrystallization in Cold-Rolled Al-Mn, Al-Sc-Zr and Al-Mn-Sc-Zr Alloy*, ADVANCED DIFFUSION PROCESSES AND PHENOMENA (eds.: Ochsner A., Murch G., Belova I.), DEFECT AND DIFFUSION FORUM 354 (2014), p. 93. DOI: 10.4028/www.scientific.net/DDF.354.93.

[P4] Vlach M., Stulikova I., Smola B. et al.: *Phase transformations in non-isothermally annealed as-cast and cold-rolled AlMnScZr alloys*, INTERNATIONAL JOURNAL OF MATERIALS RESEARCH 103 (2012) 7, p. 814. DOI: 10.3139/146.110712.

[P5] Vlach M., Smola B., Stulíková I., Očenášek V.: *Microstructure and mechanical properties of AA6082 aluminium alloy with small additions of Sc and Zr*, INTERNATIONAL JOURNAL OF MATERIALS RESEARCH 100 (2009) 3, p. 420. DOI: 10.3139/146.110022.

[P6] Vlach M., Stulíková I., Smola B., Žaludová N.: *Characterization of phase development in non-isothermally annealed mould-cast and heat-treated Al-Mn-Sc-Zr alloys*, MATERIALS CHARACTERIZATION 61 (2010) 12, p. 1400. DOI: 10.1016/j.matchar.2010.10.006.

[P7] Vlach M., Stulikova I., Smola B. et al: *Effect of cold rolling on precipitation processes in Al-Mn-Sc-Zr alloy*, MATERIALS SCIENCE AND ENGINEERING A-STRUCTURAL MATERIALS PROPERTIES MICROSTRUCTURE AND PROCESSING 548 (2012), p. 27. DOI: 10.1016/j.msea.2012.03.063.

[P8] Vlach M., Stulikova I., Smola B. et al.: *Precipitation in cold-rolled Al-Sc-Zr and Al-Mn-Sc-Zr alloys prepared by powder metallurgy*, MATERIALS CHARACTERIZATION 86 (2013), p. 59. DOI: 10.1016/j.matchar.2013.09.010.

[P9] Vlach M., Stulikova I., Smola B. et al.: *Annealing effects in hot-deformed Al-Mn-Sc-Zr alloys*, KOVOVE MATERIALY-METALLIC MATERIALS 53 (2015) 5, p. 295. DOI: 10.4149/km_2015_5_295.

[P10] Stulíková I., Smola B., Žaludová N., Vlach M., Pelcová J.: *Development of electrical resistivity due to solution treatment of squeeze cast magnesium-rare earth alloys*, KOVOVE MATERIALY-METALLIC MATERIALS 43 (2005) 4, p. 272.

[P11] Melikhova O., Cizek J., Hruska P., Vlcek M., Prochazka I., Vlach M. et al.: *Influence of Deformation on Precipitation Kinetics in Mg-Tb Alloy*, RECENT ADVANCES IN MASS TRANSPORT IN MATERIALS (eds.: Ochsner A., Belova I., Murch G. E), DEFECT AND DIFFUSION FORUM 322 (2012), p. 151. DOI: 10.4028/www.scientific.net/DDF.322.151.

[P12] Cizek J., Smola B., Stulikova I., Hruska P., Vlach M. et al.: *Natural aging of Mg-Gd and Mg-Tb alloys,* PHYSICA STATUS SOLIDI A-APPLICATIONS AND MATERIALS SCIENCE 209 (2012) 11, p. 2135. DOI: 10.1002/pssa.201228327.
[P13] Neubert V., Stulíková I., Smola B., Mordike B. L., Vlach M., Bakkar A., Pelcová J.: *Thermal stability and corrosion behaviour of Mg–Y–Nd and Mg–Tb–Nd alloys*, MATERIALS SCIENCE AND ENGINEERING A-STRUCTURAL MATERIALS PROPERTIES MICROSTRUCTURE AND PROCESSING 462 (2007), p. 329. DOI: 10.1016/j.msea.2005.11.077.
[P14] Smola B., Stulikova I., Cerna J., Cizek J., Vlach M.: *Phase transformations in MgTbNd alloy*, PHYSICA STATUS SOLIDI A-APPLICATIONS AND MATERIALS SCIENCE 208 (2011) 12, p. 2741. DOI: 10.1002/pssa.201127296.
[P15] Stulikova I., Smola B., Vlach M., Kudrnova H., Piesova J.: *Influence of powder metallurgy route on precipitation processes in MgTbNd alloy*, MATERIALS CHARACTERIZATION 112 (2016), p. 149. DOI: 10.1016/j.matchar.2015.12.020.
[P16] Čížek J., Procházka I., Smola B., Stulíková I., Vlach M. et al.: *Precipitation effects in ultra-fine-grained Mg-RE alloys*, INTERNATIONAL JOURNAL OF MATERIALS RESEARCH 100 (2009) 6, p. 780. DOI: 10.3139/146.110103.
[P17] Vlach M., Cizek J., Melikhova O., Kodetova V., Stulikova I.: *Hydrogen trapping at defects in Pd and thermally activated desorption*, DIFFUSION IN SOLIDS AND LIQUIDS X (eds.: Ochsner A., Murch G. E., Shokuhfar A., Delgado J. M. P. Q.), DEFECT AND DIFFUSION FORUM 365 (2015), p. 36. DOI: 10.4028/www.scientific.net/DDF.365.36.
[P18] Čížek J., Procházka I., Vlach M. et al.: *Hydrogen-induced buckling of Pd films studied by positron annihilation,* APPLIED SURFACE SCIENCE 255 (2008) 1, p. 241. DOI: 10.1016/j.apsusc.2008.05.290.
[P19] Cizek J., Melikhova O., Vlcek M., Lukac F., Vlach M. et al.: *Hydrogen-induced microstructural changes of Pd films*, INTERNATIONAL JOURNAL OF HYDROGEN ENERGY 38 (2013) 27, p. 12115. DOI: 10.1016/j.ijhydene.2013.03.096.
[P20] Vlcek M., Lukac F., Vlach M. et al.: *Influence of microstructure and mechanical stress on behaviour of hydrogen in 500 nm Pd films*, JOURNAL OF ALLOYS AND COMPOUNDS 645 (2015), p. S446. DOI: 10.1016/j.jallcom.2014.12.086.
[P21] Čížek J., Procházka I., Melikhova O., Vlach M. et al.: *Hydrogen-induced defects in Pd films*, PHYSICA STATUS SOLIDI C – SOLID STATE PHYSICS 6 (2009) 11, p. 2364. DOI: 10.1002/pssc.200982064.
[P22] Wagner S., Uchida H., Burlaka V., Vlach M. et al.: *Achieving coherent phase transition in palladium-hydrogen thin films*, SCRIPTA MATERIALIA 64 (2011) 10, p. 978. DOI: 10.1016/j.scriptamat.2011.02.004.
[P23] Lukac F., Vlcek M., Vlach M. et al.: *Stress release during cyclic loading of 20 nm palladium films*, JOURNAL OF ALLOYS AND COMPOUNDS 645 (2015), p. S450. DOI: 10.1016/j.jallcom.2014.12.085.